0013-7227/07/$15.00/0
Printed in U.S.A.

Endocrinology 148(3):1059–1079

doi: 10.1210/en.2006-0683

Gene Expression Profiling of the Human Maternal-Fetal Interface Reveals Dramatic Changes between Midgestation and Term

Virginia D. Winn, Ronit Haimov-Kochman, Agnes C. Paquet, Y. Jean Yang, M. S. Madhusudhan, Matthew Gormley, Kui-Tzu V. Feng, David A. Bernlohr, Susan McDonagh, Lenore Pereira, Andrej Sali, and Susan J. Fisher

Departments of Obstetrics, Gynecology, and Reproductive Sciences (V.D.W., R.H.-K., M.G.), Cell and Tissue Biology (R.H.-K., K.-T.V.F., S.M., L.P., S.J.F.), and Medicine (A.C.P., Y.J.Y.), Lung Biology Center, Departments of Biopharmaceutical Sciences and Pharmaceutical Chemistry (M.S.M., A.S.) and Anatomy and Pharmaceutical Chemistry (S.J.F.), California Institute for Quantitative Biomedical Research (M.S.M., A.S.), University of California, San Francisco, San Francisco, California 94143; and Department of Biochemistry, Molecular Biology, and Biophysics (D.A.B.), University of Minnesota, Minneapolis, Minnesota 55455

Human placentation entails the remarkable integration of fetal and maternal cells into a single functional unit. In the basal plate region (the maternal-fetal interface) of the placenta, fetal cytotrophoblasts from the placenta invade the uterus and remodel the resident vasculature and avoid maternal immune rejection. Knowing the molecular bases for these unique cell-cell interactions is important for understanding how this specialized region functions during normal pregnancy with implications for tumor biology and transplantation immunology. Therefore, we undertook a global analysis of the gene expression profiles at the maternal-fetal interface. Basal plate biopsy specimens were obtained from 36 placentas (14–40 wk) at the conclusion of normal pregnancies. RNA was isolated, processed, and hybridized to HG-U133A&B Affymetrix GeneChips. Surprisingly, there was little change in gene expression during the 14- to 24-wk interval. In contrast, 418 genes were differentially expressed at term (37–40 wk) as compared with midgestation (14–24 wk). Subsequent analyses using quantitative PCR and immunolocalization approaches validated a portion of these results. Many of the differentially expressed genes are known in other contexts to be involved in differentiation, motility, transcription, immunity, angiogenesis, extracellular matrix dissolution, or lipid metabolism. One sixth were nonannotated or encoded hypothetical proteins. Modeling based on structural homology revealed potential functions for 31 of these proteins. These data provide a reference set for understanding the molecular components of the dialogue taking place between maternal and fetal cells in the basal plate as well as for future comparisons of alterations in this region that occur in obstetric complications. (*Endocrinology* 148: 1059–1079, 2007)

SURVIVAL AND GROWTH of the fetus require normal development of the placenta, which in humans involves the formation of a transient organ with both maternal and fetal contributions. Specifically, invasive cytotrophoblasts (CTBs), components of anchoring chorionic villi, attach to and invade the maternal decidua. A subset of these cells remodel the uterine vasculature, which they also occupy (Fig. 1). This process primarily occurs during the second trimester of pregnancy. The region in which maternal and fetal cells coexist is termed the basal plate or maternal-fetal interface, and its proper formation and function are required for normal pregnancy outcome. At a cellular level, many unusual processes occur in this area. For example, invasive CTBs execute a novel epithelial-to-mesenchymal transition that enables vascular mimicry (1, 2). Perhaps most remarkably, the maternal immune system tolerates the invasion of the hemiallogeneic fetal cells for the duration of pregnancy.

First Published Online December 14, 2006

Abbreviations: ANGPT-2, Angiopoietin-2; CK, cytokeratin; CTB, cytotrophoblast; FABP4, fatty acid binding protein 4; GO, gene ontogeny; IPA, Ingenuity Pathway Analysis; LPL, lipoprotein lipase; MCPH1, microcephalin; NK, natural killer; Q-PCR, quantitative PCR.

***Endocrinology* is published monthly by The Endocrine Society (http://www.endo-society.org), the foremost professional society serving the endocrine community.**

Over the past several decades, a great deal of information has been gained about placental development by taking a candidate molecule approach (3). By analogy with cells and tissues that perform similar functions in other contexts, progress has been made toward understanding many components of placental development. For example, the fact that endovascular CTBs function as endothelial cells prompted investigators to study the role of vasculogenic/angiogenic molecules, including adhesion receptors, at the maternal-fetal interface (4, 5). As in many tumors, CTBs use matrix metalloproteinases for the purpose of invasion (6, 7). However, there are also numerous examples of seemingly novel mechanisms that are unique to placental development. For example, trophoblasts in all locations lack major histocompatibility class II expression, and upon allocation to the invasive pathway, CTBs upregulate human leukocyte antigen-G, a nonclassical major histocompatibility class I molecule, in the absence of human leukocyte antigen-A and -B expression (8, 9). Accordingly, unbiased analyses, such as microarray approaches, are also crucial for obtaining new insights into the mechanisms that are required for normal basal plate formation and function during pregnancy.

As in many research areas, genome-wide expression profiling approaches are being used to understand trophoblast

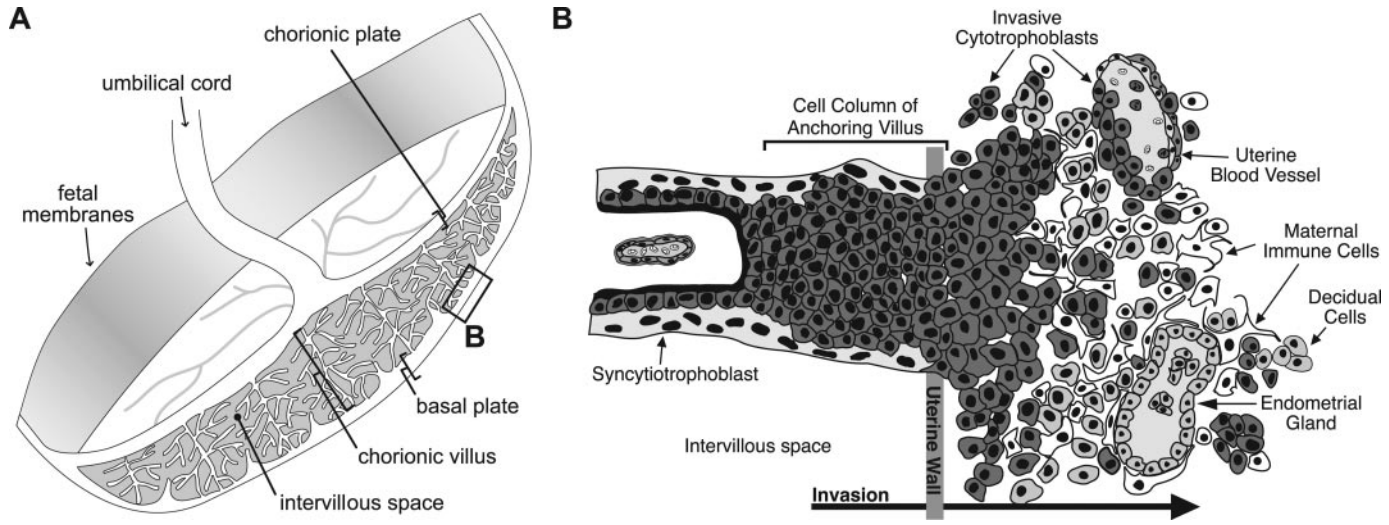

FIG. 1. Diagram of the human maternal-fetal interface. A, Representation of the human placenta after delivery. The placental surface that was adjacent to the uterine wall is termed the basal plate. The *boxed area* denotes the region biopsied for these studies. B, View of the basal plate at the cellular level. This chimeric region of the placenta is composed of both maternal and fetal components: extravillous (invasive) cytotrophoblasts (*dark gray*), decidual cells (*light gray*), remodeled vasculature (both invasive CTBs and maternal endothelium) and maternal immune cells (*white*).

differentiation and placental development. Several types of experimental designs have been published. Aronow *et al.* (10) characterized human term CTB syncytialization and the role of the activator protein 2α transcription factor in this process (11). Kudo *et al.* (12) also studied syncytialization but focused on the BeWo line rather than on primary cells. Roh *et al.* (13) analyzed the effects of hypoxia on human term trophoblasts, which led to their most recent work showing a role for *N*-myc-down-regulated gene 1 (14). In addition, there are several published reports that describe the gene expression patterns of the placenta as a whole. Tanaka *et al.* (15) used a microarray approach to compare the genetic bases of murine placental and embryonic development at midgestation and subsequently validated and extended the results (16). Hemberger *et al.* (17) focused on the murine extraembryonic tissues together with the adjacent decidua at d 7.5, compared with d 17.5.

The Hemberger study design took into consideration that trophoblast-decidual interactions are critical determinants of pregnancy outcome. For this reason, we used the same basic strategy, profiling gene expression at the human maternal-fetal interface during five gestational age intervals: 14–16, 18–19, 21, 23–24, and 37–40 wk. RNA was isolated from the basal plate and processed to produce samples that were hybridized to high-density, short-oligonucleotide microarrays (GeneChips HG-U133A and HG-U133B; Affymetrix, Santa Clara, CA). Very few alterations in gene expression were observed during the midgestation period (14–24 wk). In contrast, hundreds of changes, including the expression of genes known to be up- or down-regulated over gestation, were modulated between midgestation and term (37–40 wk). These data allowed us to identify molecules that play potentially important roles in the formation and function of the maternal-fetal interface.

Materials and Methods

Tissue collection

The University of California, San Francisco (UCSF), Committee on Human Research approved the tissue procurement protocol. Informed consent was obtained from each parturient before delivery. Basal plate biopsy specimens of the maternal-fetal interface from second- and third-trimester placentas [gestational ages 14–16 wk (n = 6), 18–19 wk (n = 9), 21 wk (n = 6), 23–24 wk (n = 6), and 37–40 wk (n = 9)] were collected. Second-trimester samples were obtained after elective terminations of singleton pregnancies. The products of terminations performed for fetal indications, infection, or maternal health complications were excluded. Term samples were collected after cesarean delivery at the conclusion of normal nonlabored singleton pregnancies. Pregnancies complicated by fetal anomalies, hypertension, diabetes, or other significant maternal health issues were excluded. Gestational age was determined during the second trimester by measuring foot length (18) and at term by using standard dating criteria (19). The basal plate was dissected from the placenta proper, rinsed in PBS and diced into approximately 3×3 mm^3 pieces, which were snap frozen in liquid nitrogen and stored at -70 C. All samples were processed and frozen within 1 h of delivery. For immunohistochemistry, biopsy samples of the basal plate were fixed in 3% paraformaldehyde in PBS (wt/vol), passed through a sucrose gradient (5–15% in PBS), and frozen in optimal cutting temperature.

In addition, biopsies of several regions of the tissue were also fixed in 10% neutral-buffered formalin and embedded in paraffin. Tissue sections prepared from the blocks were stained with hematoxylin and eosin and examined by using a light microscope. In all cases, normal morphological features were noted; there were no histological signs of placental or decidual pathology.

Total RNA extraction

RNA was isolated from snap-frozen basal plate specimens using a modified Trizol method that was developed during the course of this work (20). Briefly, homogenization of 0.9–1 g of frozen basal plate specimens was carried out in 10 ml of cold Trizol reagent (Invitrogen, Frederick, MD) on wet ice (0–4 C). Cellular debris was pelleted by centrifugation at 12,000 $\times$ *g* for 10 min. Then the supernatant was transferred to Phase Lock Gel heavy tubes (Eppendorf, Netheler, Germany), and RNA was isolated according to the manufacturer's instructions. The total RNA fraction was purified further by using an RNeasy mini kit (QIAGEN, Valencia, CA) according to the manufacturer's in-

structions. Aliquots of the RNA isolated from the specimens were evaluated by using the Agilent RNA 6000 Nano LabChip kit (Agilent Technologies, Amstelveen, The Netherlands) on an Agilent Bioanalyzer 2100 system using the nano assay for eukaryote total RNA. Capillary electrophoresis data in commaseparated value files were analyzed by using the Degradometer version 1.41 software (available at www.dnaarrays.org) (21). Only RNA with a degradation factor of less than 11 was used in subsequent microarray experiments.

Microarray hybridization

The microarray platform was the high-density HG-U133A and HG-U133B GeneChips (Affymetrix) that use 45,000-oligomer probe sets representing 39,000 transcripts. Hybridization was accomplished by using the protocol devised by the UCSF Gladstone (National Heart, Lung, and Blood Institute) Genomics Core Facility (www.gladstone.ucsf.edu/gladstone/php/section). In brief, double-stranded cDNAs were generated from total RNA samples by using SuperScript II reverse transcriptase (Invitrogen) and a T7-oligo primer (QIAGEN). Biotin-labeled cRNA was synthesized by *in vitro* transcription using an Enzo Bioassay RNA labeling kit (Enzo Diagnostics, Farmingdale, NY). The labeled cRNA was purified with an RNeasy column (QIAGEN). Before hybridization, the quality of all *in vitro* transcription products was evaluated by using the Agilent Bioanalyzer 2100 system. Then the cRNA was fragmented at 94 C for 35 min in buffer [Tris-acetate 40 mmol/liter, potassium acetate 100 mmol/liter, magnesium acetate 30 mmol/liter (pH 8.1)]. Samples from individual basal plates were analyzed separately. Specifically, the HG-U133A and HG-U133B Affymetrix GeneChips were each hybridized with 15 μg of cRNA and then washed, stained, and imaged at the Gladstone Genomics Core Facility by using standard Affymetrix protocols. Data files were deposited in the Gene Expression Omnibus data repository with accession no. GSE5999.

Data analysis

The raw image data were analyzed by using GeneChip Expression Analysis software (Affymetrix) to produce perfect match and mismatch values. Subsequently quality control, preprocessing, and linear modeling were performed using Bioconductor (22), an open-source and open-development software project based on the R statistical package (www.r-project.org). Clustering analysis was performed using Acuity software (Molecular Devices Corp., Sunnyvale, CA). Initial hybridization quality was assessed by using Bioconductor package affyPLM, and the slight variations in quality were compensated for during the preprocessing stage, which was performed in two steps. First, we used a Probe Level robust linear model (23) to obtain separate normalized log intensities for each chip (*i.e.* background subtraction, quantile normalization, and probe set summarization). Second, we applied a global median normalization at the probe set level to all A and B GeneChips (n = 72) and then combined these data into a matrix of $\log_2$-based gene expression measures, in which columns corresponded to different cRNA samples, and rows corresponded to the different probe sets.

Initial analyses showed that gene expression during the second-trimester intervals was stable. Therefore, subsequent analyses were performed by comparing the gene expression data from the midgestation samples (14–24 wk; n = 27) with those obtained at term (37–40 wk; n = 9). Estimated log ratios (M value) between term and midgestation were determined by using the limma software package in R (24). Then differentially expressed genes were selected by determining the moderated *t* statistic-adjusted *P* values (<0.05 using Bonferroni correction). The results showed that the expression of 418 genes (505 probe sets) was significantly modulated. Then the normalized intensity values for this data set were centered to the median intensity value for each probe set, after which the probe sets were ranked according to their M values (representing fold change) and depicted as a gene expression color map.

The gap statistic with Euclidean distance was used to select the cluster number (k = 11) for subsequent application of the K-means algorithm (25). Then differentially expressed genes from each cluster were presented as a hierarchical dendogram of the normalized log intensity data based on the Euclidean squared metric and average linkage. This analysis enabled us to visually evaluate both transcript levels and patterns of coregulation.

Pathway and network analysis

Initially, gene ontogeny (GO) annotations were determined (www.genetools.microarray.ntnu.no) and used to categorize the differentially expressed genes according to the biological processes in which they were involved (level 2). When biological process information was lacking, genes were annotated according to molecular function. To determine whether there was a significant overrepresentation of differentially expressed genes in particular functions or physiologic processes, the data set was analyzed by using Ingenuity Pathway Analysis 3.1 software (www.ingenuity.com). The data set containing gene identifiers and their corresponding expression values was uploaded as an Excel spreadsheet using the template provided in the application. Each gene identifier was mapped to its corresponding gene object in the Ingenuity Pathways Knowledge Base. Differentially regulated genes, identified by using an adjusted $P < 0.05$ as the cut-off, were then used as the starting point for generating biological networks.

Specifically, all the differentially expressed genes as well as the subset that exhibited more than a 2-fold change in expression were evaluated according to their molecular and cellular functions and the physiological processes in which they participated. In addition, their participation in metabolic and signaling pathways was assessed. Finally, the differentially expressed genes were subjected to network analysis.

Quantitative PCR

RT of basal plate (total) RNA was carried out by using the TaqMan Gold RT-PCR kit (Applied Biosystems, Foster City, CA) as described by the manufacturer, followed by real-time PCR, performed in triplicate by using the Applied Biosystems 9700HT sequence detection system. All templates were amplified by using Assay-on-Demand kits (Applied Biosystems) or primer/probe sets designed by the UCSF Biomolecular Research Center (see supplemental Table 1, published as supplemental data on The Endocrine Society's Journals Online web site at http://endo.endojournals.org). Briefly, 5 μl of cDNA was added to 20 μl of 1× TaqMan Universal PCR master mix containing AmpErase UNG and 1 μl of a primer/probe. Negative controls contained either RNA that was not reverse transcribed or lacked template inputs. Reactions were incubated at 50 C for 2 min and then 95 C for 10 min, followed by 40 cycles of 95 C for 15 sec and 60 C for 1 min. Relative quantification was determined by using the standard curve method (see Applied Biosystems user bulletin no. 2; www.appliedbiosystems.com). In preliminary experiments, we investigated the utility of 11 potential targets as endogenous controls (endogenous control plate; Applied Biosystems). The results showed that the 18S rRNA did not vary with gestational age. Accordingly, the levels of this transcript were used to obtain normalized values for the target amplicons. Then these values were calibrated to a 14-wk sample, the earliest gestational age included in our analysis. Results were reported as the relative fold mRNA levels ± SD for each basal plate specimen. The means of the term and midgestation samples were compared using a two-tailed Student's *t* test ($P < 0.05$).

Immunohistochemistry

Frozen sections (5 μM) cut from optimal cutting temperature-embedded tissues were washed in PBS and nonspecific reactivity was blocked with 3% BSA, 0.1% Triton X-100, and 0.5% Tween 20 in PBS for 30 min. Then the experimental sections were incubated with mouse antihuman lipoprotein lipase (LPL) antibody (1:100; 5D2; the kind gift of John Brunzell, University of Washington, Seattle, WA) for 1 h, after which they were washed in PBS three times for 5 min. Negative controls were incubated in the absence of the primary antibody. Then both experimental and control sections were incubated in rat antihuman cytokeratin antibody (CK) [1:100; 7D3 (26)]) for 1 h and washed in PBS as described above. To localize the bound primary antibodies, the sections were incubated with Alexa Fluor 594-conjugated goat antimouse IgG (1:1000; Molecular Probes Inc., Eugene, OR) and fluorescein isothiocyanate-labeled donkey antirat IgG (1:200; Jackson ImmunoResearch Laboratories, West Grove, PA) antibodies for 30 min and washed again in PBS. Tissue sections were mounted in Vectashield containing 4′-6-diamidino-2-phenylindol (Vector Laboratories, Burlingame, CA), which allowed visualization of the nuclei. Immunoreactivity was imaged using a Leica DM 5000B fluorescent microscope equipped with a Leica DFC 350FX digital camera (Leica Instruments, San Jose, CA).

Expression of fatty acid binding protein 4 (FABP4) in the basal plate was evaluated by using a rabbit antimurine polyclonal antibody that specifically reacted with this protein (27). The immunostaining protocol was identical with that described for LPL except that the primary antibody was at a 1:1000 dilution and the secondary antibody was Alexa Fluor 594-conjugated goat antirabbit IgG (1:1000; Molecular Probes).

Protein function annotation by sequence homology and structural similarity

To determine the function of the differentially expressed genes that lacked annotations (www.genetools.microarray.ntnu.no; July 2005), we used protein sequence homology searches along with protein structure modeling. Briefly, protein sequences for the differentially expressed genes were extracted by using their UniGene identifiers (28). Homology searches were done using PSI-BLAST (29). Five iterations of the PSI-BLAST were run using an e-value cutoff of 10^{-5} for sequences to be included in the profile. For protein sequences with detectable homology to other proteins of known structure, comparative structure models were built through the MODWEB server (30), which uses the program MODELLER (31). The resulting models were deposited in the model database MODBASE (32). Proteins that could not be assigned a function based on homology searches were subjected to threading using the mGenTHREADER software (33).

Results

Gene expression patterns at the maternal-fetal interface change dramatically between second trimester and term

First, we determined the gene expression profiles of 36 human basal plate samples that were collected between the gestational ages of 14 and 40 wk. The relevant clinical data pertaining to each specimen are presented as supplemental data (supplemental Table 2). Pair-wise comparisons between each of the five gestational age intervals showed remarkably stable patterns of gene expression among the second trimester arrays (14–24 wk). In contrast, numerous differences were observed between midgestation (14–24 wk) and term (37–40 wk). The differentially expressed transcripts, a total of 418 genes/expressed sequence tags (505 probe sets), were identified. Statistical analysis of maternal age and parity showed that there were no significant differences in these parameters between the RNA samples that were prepared from midgestation and term basal plate biopsies.

An MA scatter-plot that depicts the fold change and signal intensity for every probe set is presented as supplemental data (supplemental Fig. 1). The differentially expressed genes normalized to the median value and ordered by their fold change are shown as a heat map in Fig. 2A. The areas that contain the 35 most highly up- or down-regulated probe sets have been enlarged and annotated (Fig. 2B, *upper* and *lower panels*, respectively). Annotation of the complete heat map is provided as supplemental data (supplemental Fig. 2). The entire set of genes that were up-regulated at term is summarized in Table 1, where they are also categorized according to the biological processes in which they participate or their molecular functions based on the relevant GO annotation (www.genetools.microarray.ntnu.no). The probe set identifier, gene symbol, GO annotation, and fold change are also included in Table 1. Table 2 presents analogous information concerning the genes that were down-regulated at term. As expected, genes with known expression patterns, either up-regulated [*e.g.* CRH (34) and inhibin-βA subunit (35)] or down-regulated [*e.g.* C-X-C chemokine ligand 14 (36) and angiopoietin-2 (ANGPT-2) (5)] at term, were present in the data set.

Coregulation of differentially expressed genes

To examine patterns of coexpression and possibly coregulation, we performed K-means cluster analysis. Cluster sizes ranged from 4 to 121 probe sets. Five clusters contained up-regulated genes and six clusters contained down-regulated genes. Examples of the clusters (n = 4) created are shown as heat maps that were constructed by hierarchical clustering of the log intensity data (Fig. 3). The remaining clusters (n = 7) are available as supplemental data (supplemental Fig. 3). Cluster A is composed of four probe sets for two genes, ANGPT-2 and microcephalin (MCPH1; formerly hypothetical protein FLJ12847). The Pearson correlation coefficients among these four probe sets were extremely high (0.92–0.97), suggesting very tight coregulation. On further examination, the chromosomal location for both genes was found to be 8p23.1, in which they are transcribed from the same DNA sequence in opposite directions. Cluster B contains the most highly up-regulated genes: LPL, FABP4, CRH, HBB, and ALPP. Cluster C includes a significant proportion of genes with immunological functions that are regulated in a similar manner. Finally, cluster D contains numerous genes that encode proteins with unknown functions.

Differentially expressed genes: functions, pathways, and networks

The GO annotations suggested that the differentially expressed genes were involved in a variety of biological processes. At least one sixth were expressed sequence tags or hypothetical proteins and thus were not annotated. Of the known differentially expressed genes, 17 were related to lipid metabolism, 10 were involved with formation or regulation of the extracellular matrix, 21 were immune effectors or modulators, 24 were transcription factors, and six had angiogenic/vasculogenic functions. Interestingly, of the 39 genes that were involved in signal transduction, five functioned in the Wnt-β-catenin pathway (FRAT1, CTNNBIP1, DKK1, SFRP1, and KREMEN1).

The GO annotations indicated that the differentially expressed genes within the basal plate region were involved in a variety of specific functions and biological processes. Thus, we used Ingenuity Pathway Analysis (IPA) to determine the significance of these observations. IPA showed that 23 molecular functions and 22 physiologic processes included more differentially expressed genes than would be expected by chance ($-\log$ [significance] of > 1.25, which corresponds to a $P < 0.05$; see www.ingenuity.com). These results, summarized by functional categories, are shown as supplementary data (supplemental Fig. 4). Genes that had at least a 2-fold change in expression were most significantly represented in the following categories: cell movement, cell-cell signaling, cell death, lipid metabolism, small molecule biochemistry, and gene expression.

Next, we used the IPA software to further evaluate the participation of the differentially expressed genes of the human basal plate in metabolic and signaling pathways (supplemental Table 3). Analysis of genes with at least a 2-fold change highlighted two metabolic pathways: folate biosynthesis and *N*-glycan degradation involving mannose-con-

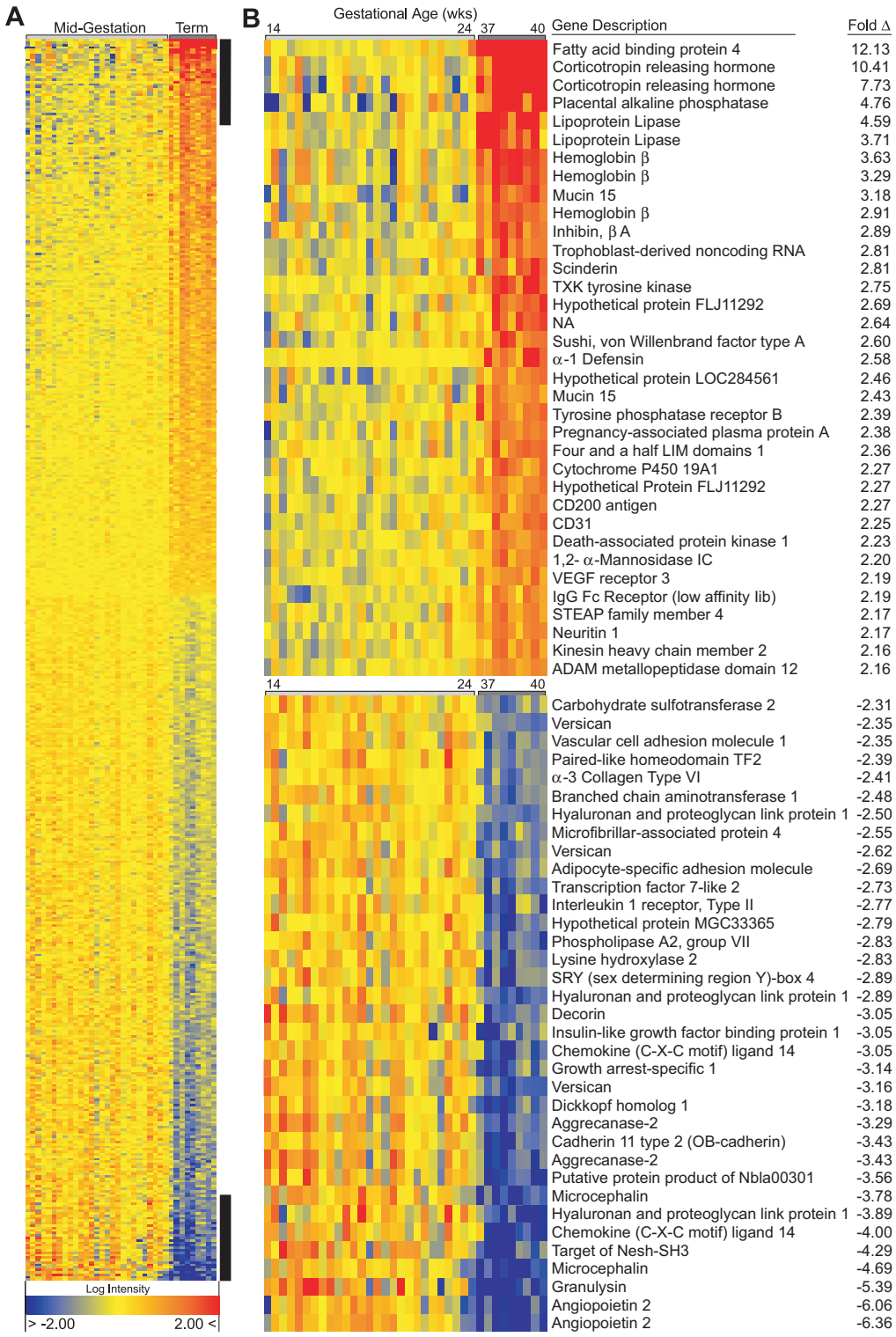

FIG. 2. Heat map of differentially expressed genes. A, The normalized log intensity values for all 505 differentially expressed probe sets were centered to the median value of each probe set and colored on a range of −2 to +2. *Red* denotes up-regulated, *yellow* denotes intermediate, and *blue* denotes down-regulated expression levels as compared with the median value. *Columns* contain data from a single basal plate specimen, and *rows* correspond to a single probe set. Samples are arranged from left to right, ordered by increasing gestational age. *Rows* are ranked by fold change [mean term value (n = 9) divided by mean midgestation value (n = 27)]. B, The most highly up-regulated (*upper panel*) and down-regulated (*lower panel*) probe sets at term were enlarged and annotated with the gene name and the fold change value. An annotated heat map of all 505 probe sets is available as supplemental data (supplemental Fig. 2).

taining structures. With regard to signaling, the differentially expressed genes were significantly overexpressed in the Wnt-β-catenin (supplemental Fig. 5) and TGF-β pathways. Finally, several other pathways were just below the 1.25 threshold, namely peroxisome proliferative activated receptor and IL-6.

We also used the IPA software to map networks of the differentially expressed genes at the human basal plate. The largest network contained genes that were involved in cell motility, cell-to-cell signaling/interaction, and tissue development. Diagrams of these networks are shown as supplementary data (supplemental Fig. 6).

TABLE 1. Differentially expressed genes upregulated at term, compared with midgestation

Identifier	Symbol	Gene ontogeny (biological process, molecular function)[a]	Fold Δ
Angiogenesis			
209498_at	CEACAM1	Angiogenesis	1.84
226028_at	ROBO4	Angiogenesis	1.69
Apoptosis/cell death			
203139_at	DAPK1	Apoptosis	2.23
225078_at	EMP2	Cell death	2.01
202695_s_at	STK17A	Apoptosis	1.57
203684_s_at	BCL2	Antiapoptosis	1.38
Carbohydrate metabolism			
218918_at	MAN1C1	Carbohydrate metabolism	2.20
205960_at	PDK4	Glucose metabolism	1.83
202032_s_at	MAN2A2	Carbohydrate metabolism	1.31
Cell adhesion			
204943_at	ADAM12	Cell adhesion	2.16
201984_s_at	EGFR	Cell-cell adhesion	1.87
209543_s_at	CD34	Cell adhesion	1.80
Cell cycle			
210511_s_at	INHBA	Cell cycle arrest	2.89
205011_at	LOH11CR2A	Cell cycle	1.60
212415_at	SEPT6	Cell cycle	1.44
209805_at	PMS2	Cell cycle	1.39
209375_at	XPC	Nucleotide-excision repair	1.23
Cell differentiation			
214505_s_at	FHL1	Cell differentiation	2.36
206176_at	BMP6	Cell differentiation	1.66
206453_s_at	NDRG2	Cell differentiation	1.53
209159_s_at	NDRG4	Cell differentiation	1.25
Cell motility/cytoskeleton			
203087_s_at	KIF2	Microtubule-based movement	2.16
221042_s_at	CLMN	Actin binding	1.91
205054_at	NEB	Regulation of actin filament length	1.77
201497_x_at	MYH11	Muscle development	1.71
215189_at	KRTHB6	Cytoskeleton organization and biogenesis	1.68
203407_at	PPL	Keratinization	1.62
242445_at	FGD4	Cytoskeleton organization and biogenesis	1.39
213711_at	KRTHB1	Structural molecule activity	1.39
Coagulation/complement			
205479_s_at	PLAU	Blood coagulation	1.88
202112_at	VWF	Platelet activation	1.64
202877_s_at	C1QR1	Cell-cell adhesion	1.56
Immune/inflammatory response			
205629_s_at	CRH	Immune response	10.41
214657_s_at	TncRNA	Immune response	2.81
205033_s_at	DEFA1	Defense response to bacteria	2.58
210889_s_at	FCGR2B	Immune response	2.19
210029_at	INDO	Immune response	1.69
823_at	CX3CL1	Immune response	1.20
Lipid metabolism			
203980_at	FABP4	Fatty acid binding	12.13
203548_s_at	LPL	Fatty acid metabolism	4.59
202345_s_at	FABP5	Lipid metabolism	2.07
206210_s_at	CETP	Lipid metabolism	1.69
205759_s_at	SULT2B1	Lipid metabolism	1.47
203896_s_at	PLCB4	Lipid catabolism	1.22
Protein biosynthesis/metabolism			
201982_s_at	PAPPA	Proteolysis and peptidolysis	2.38
225516_at	SLC7A2	Amino acid metabolism	1.93
200629_at	WARS	Protein biosynthesis	1.82
202965_s_at	CAPN6	Proteolysis and peptidolysis	1.78
219452_at	DPEP2	Proteolysis and peptidolysis	1.78
232080_at	HECW2	Ubiquitin cycle	1.77
219081_at	ANKHD1	Negative regulation of translational initiation	1.69
201100_s_at	USP9X	Ubiquitin cycle	1.49
203748_x_at	RBMS1	Regulation of translation	1.41
242846_at	KIAA1217	Protein amino acid glycosylation	1.34
220866_at	ADAMTS6	Proteolysis and peptidolysis	1.33
219923_at	TRIM45	Protein ubiquitination	1.30
Signaling			
206828_at	TXK	Intracellular signaling cascade	2.75
230250_at	PTPRB	Protein amino acid dephosphorylation	2.39

TABLE 1. *Continued*

Identifier	Symbol	Gene ontogeny (biological process, molecular function)[a]	Fold Δ
208983_s_at	PECAM1	Signal transduction	2.25
210316_at	FLT4	Protein tyrosine kinase signaling pathway	2.19
216218_s_at	PLCL2	Intracellular signaling cascade	2.13
219026_s_at	RASAL2	Signal transduction	1.74
212951_at	GPR116	Signal transduction	1.66
203911_at	RAP1GA1	Signal transduction	1.58
205458_at	MC1R	Signal transduction	1.54
213592_at	AGTRL1	Signal transduction	1.48
230800_at	ADCY4	Intracellular signaling cascade	1.47
222537_s_at	CDC42SE1	Signal transduction	1.47
221489_s_at	SPRY4	Regulation of signal transduction	1.44
220901_at	GPR157	G protein-coupled receptor protein signaling pathway	1.43
209110_s_at	RGL2	Ras protein signal transduction	1.42
229910_at	SHE	Intracellular signaling cascade	1.39
218950_at	CENTD3	Signal transduction	1.36
203081_at	CTNNBIP1	Signal transduction	1.29
219889_at	FRAT1	Wnt receptor signaling pathway	1.29
229055_at	GPR68	Inflammatory response signal transduction	1.21
Steroid biosynthesis			
204818_at	HSD17B2	Estrogen biosynthesis	2.14
Transcription			
232292_at	ZNF100	Regulation of transcription, DNA dependent	2.27
213541_s_at	ERG	Transcription	1.97
206059_at	ZNF91	Transcription	1.92
227198_at	AFF3	Regulation of transcription, DNA dependent	1.91
219371_s_at	KLF2	Transcription	1.85
210426_x_at	RORA	Transcription	1.47
205247_at	NOTCH4	Transcription	1.47
232286_at	AFF3	Regulation of transcription, DNA dependent	1.38
203451_at	LDB1	Negative regulation of transcription, DNA dependent	1.32
204754_at	HLF	Transcription	1.27
223714_at	ZNF256	Transcription	1.26
207164_s_at	ZNF238	Transcription	1.25
Transport			
209116_x_at	HBB	Oxygen transport	3.63
225987_at	STEAP4	Electron transport	2.17
239459_s_at	CYP19A1	Electron transport	2.10
214734_at	EXPH5	Intracellular protein transport	2.07
227123_at	RAB3B	Intracellular protein transport	1.96
206834_at	HBD	Oxygen transport	1.73
225259_at	RAB6B	Intracellular protein transport	1.58
209237_s_at	SLC23A2	Nucleobase transport	1.56
218744_s_at	PACSIN3	Endocytosis	1.54
212807_s_at	SORT1	Endocytosis	1.52
205866_at	FCN3	Phosphate transport	1.51
236982_at	PTTG1IP	Protein import into nucleus development	1.34
217683_at	HBE1	Oxygen transport	1.23
206775_at	CUBN	Cobalamin transport	1.16
Other			
204664_at	ALPP	Metabolism	4.76
218625_at	NRN1	Neuritogenesis	2.17
212327_at	KIAA1102	Smooth muscle contraction	2.00
212277_at	MTMR4	Protein amino acid dephosphorylation	1.92
204249_s_at	LMO2	Development	1.66
205464_at	SCNN1B	Sensory perception	1.65
225467_s_at	RDH13	Metabolism	1.65
209074_s_at	TU3A	Regulation of cell growth	1.64
201913_s_at	COASY	Coenzyme A biosynthesis	1.57
212266_s_at	SFRS5	Nuclear mRNA splicing, via spliceosome	1.56
226599_at	KIAA1727	Cell organization and biogenesis	1.51
203099_s_at	CDYL	Chromatin assembly or disassembly	1.43
202479_s_at	TRIB2	Protein amino acid phosphorylation	1.42
214607_at	PAK3	Protein amino acid phosphorylation	1.40
204153_s_at	MFNG	Pattern specification	1.38
232852_at	LDB2	Development	1.34
221486_at	ENSA	Response to nutrients	1.33
206793_at	PNMT	Catecholamine biosynthesis	1.33
205950_s_at	CA1	One-carbon compound metabolism	1.28
232852_at	LDB2	Development	1.34

TABLE 1. *Continued*

Identifier	Symbol	Gene ontogeny (biological process, molecular function)[a]	Fold Δ
Unknown			
227241_at	MUC15		3.18
239365_at	SCIN		2.81
213247_at	SVEP1		2.14
209343_at	EFHD1		2.03
210295_at	MAGEA10		1.73
227923_at	SHANK3		1.73
219091_s_at	EMILIN3		1.67
205093_at	PEPP3		1.64
226907_at	PPP1R14C		1.64
229598_at	COBLL1		1.59
219280_at	WDR9		1.55
243594_x_at	Spir-2		1.49
229604_at	CMAH		1.47
55616_at	CAB2		1.45
210751_s_at	RGN		1.42
204761_at	USP6NL		1.38
228679_at	PHYHIPL		1.36
226499_at	TUBB2		1.32
219233_s_at	GSDML		1.31
219265_at	MOBKL2B		1.29
233520_s_at	CMYA5		1.26
212261_at	TNRC15		1.26
220065_at	TNMD		1.25
Hypothetical proteins			
215187_at	FLJ11292		2.69
233737_s_at	LOC284561		2.46
225316_at	FLJ14490		2.13
219721_at	FLJ11181		2.07
228568_at	FLJ30973		1.73
218546_at	FLJ14146		1.61
220003_at	FLJ11004		1.56
222760_at	FLJ14299		1.52
226599_at	KIAA1727		1.51
223203_at	PRO0659		1.48
217795_s_at	MGC3222		1.46
229144_at	KIAA1026		1.46
212957_s_at	LOC92249		1.45
243017_at	LOC158572		1.39
242417_at	LOC283278		1.38
230277_at	LOC442602		1.35
236266_at	LOC283666		1.32
226735_at	FLJ90013		1.27
219881_s_at	FLJ23053		1.20
ORF			
221766_s_at	C6orf37		1.64
220456_at	C20orf38		1.61
225499_at	C20orf74		1.59
232300_at	C10orf116		1.57
231991_at	C20orf160		1.47
230254_at	C6orf188		1.39
Nonannotated			
239365_at	NA		2.81
221200_at	NA		2.64
213929_at	NA		2.08
231644_at	NA		1.87
226964_at	NA		1.84
236765_at	NA		1.71
229380_at	NA		1.49
239319_at	NA		1.43
229201_at	NA		1.40
236657_at	NA		1.39
242909_at	NA		1.38
227780_s_at	NA		1.36
240923_at	NA		1.35
243242_at	NA		1.34
231047_at	NA		1.32
214076_at	NA		1.32
235877_at	NA		1.27

ORF, Open reading frame.
[a] Obtained from www.genetools.microarray.ntnu.no as of March 2006.

TABLE 2. Differentially expressed genes down-regulated at term, compared with midgestation

Identifier	Symbol	Gene ontogeny (biological process, molecular function)[a]	Fold Δ
Amino acid metabolism			
203560_at	GGH	Glutamine metabolism	2.17
201599_at	OAT	Amino acid metabolism	2.03
207076_s_at	ASS	Amino acid biosynthesis	1.92
215001_s_at	GLUL	Glutamine biosynthesis	1.73
219933_at	GLRX2	Glutathione metabolism	1.46
Angiogenesis			
205572_at	ANGPT2	Angiogenesis	6.36
202283_at	SERPINF1	Negative regulation of angiogenesis	1.57
204575_s_at	MMP19	Angiogenesis	1.56
213001_at	ANGPTL2	Development	1.42
Apoptosis			
218856_at	TNFRSF21	Apoptosis, signal transduction	1.80
202123_s_at	ABL1	Signal transduction resulting in induction of apoptosis	1.48
208822_s_at	DAP3	Apoptosis	1.34
Carbohydrate metabolism			
221760_at	MAN1A1	Carbohydrate metabolism	2.17
203343_at	UGDH	Glycosaminoglycan biosynthesis	2.07
221024_s_at	SLC2A10	Carbohydrate transport	2.06
201193_at	IDH1	Carbohydrate metabolism	1.85
200650_s_at	LDHA	Anaerobic glycolysis	1.65
201576_s_at	GLB1	Carbohydrate metabolism	1.59
224915_x_at	TALDO1	Carbohydrate metabolism	1.47
201425_at	ALDH2	Carbohydrate metabolism	1.46
202847_at	PCK2	Gluconeogenesis	1.24
Cell adhesion			
205523_at	HAPLN1	Cell adhesion	3.89
207173_x_at	CDH11	Homophilic cell adhesion	3.43
212713_at	MFAP4	Cell adhesion	2.55
201438_at	COL6A3	Cell adhesion	2.41
203868_s_at	VCAM1	Cell-cell adhesion	2.35
209436_at	SPON1	Cell adhesion	1.89
228233_at	FREM1	Homophilic cell adhesion	1.32
Cell cycle			
204457_s_at	GAS1	Cell cycle	3.14
202769_at	CCNG2	Cell division	2.03
209773_s_at	RRM2	DNA replication	1.82
227280_s_at	FLJ40432	Regulation of cell cycle	1.75
202907_s_at	NBN	Telomere maintainence; DNA repair	1.74
213093_at	PRKCA	Regulation of progression through cell cycle	1.72
203625_x_at	SKP2	Regulation of progression through cell cycle	1.72
201930_at	MCM6	Cell cycle	1.67
213864_s_at	NAP1L1	DNA replication	1.59
214710_s_at	CCNB1	Cell division	1.59
202330_s_at	UNG	Base-excision repair	1.43
Cell motility/cytoskeleton			
208636_at	ACTN1	Structural constituent of cytoskeleton	1.95
209191_at	TUBB6	Microtubule-based movement	1.80
212320_at	TUBB	Microtubule-based movement	1.59
243_g_at	MAP4	Negative regulation of microtubule depolymerization	1.42
200609_s_at	WDR1	Perception of sound	1.39
201462_at	SCRN1	Exocytosis	1.36
219431_at	ARHGAP10	Cytoskeleton organization and biogenesis	1.28
Extracellular matrix			
204619_s_at	CSPG2	Cell recognition	3.16
201744_s_at	LUM	Collagen fibril organization	2.23
204114_at	NID2	Cell-matrix adhesion	2.20
202465_at	PCOLCE	Development	2.11
203325_s_at	COL5A1	Cell adhesion	2.08
209711_at	SLC35D1	Chondroitin sulfate biosynthesis	2.04
215076_s_at	COL3A1	Organogenesis	1.87
213428_s_at	COL6A1	Cell adhesion	1.80
221729_at	COL5A2	Phosphate transport	1.68
218927_s_at	CHST12	Dermatan sulfate biosynthesis	1.38
Immune/inflammatory response			
37145_at	GNLY	Cellular defense response	5.39
218002_s_at	CXCL14	Inflammatory response	4.00
205403_at	IL1R2	Immune response	2.77

TABLE 2. *Continued*

Identifier	Symbol	Gene ontogeny (biological process, molecular function)[a]	Fold Δ
203921_at	CHST2	Inflammatory response	2.31
200986_at	SERPING1	Immune response	2.25
209875_s_at	SPP1	Immune cell chemotaxis	2.16
206584_at	LY96	Inflammatory response	1.92
266_s_at	CD24	Humoral immune response	1.88
205291_at	IL2RB	Immune response	1.79
203717_at	DPP4	Immune response	1.74
225646_at	CTSC	Immune response	1.72
232224_at	MASP1	Immune response	1.58
217947_at	CKLFSF6	Chemotaxis	1.57
205098_at	CCR1	Inflammatory response	1.46
Lipid metabolism			
206214_at	PLA2G7	Lipid catabolism	2.83
203335_at	PHYH	Lipid metabolism	1.97
206726_at	PGDS	Fatty acid biosynthesis	1.85
200832_s_at	SCD	Fatty acid biosynthesis	1.79
211070_x_at	DBI	Transport	1.77
202068_s_at	LDLR	Lipid metabolism	1.73
208962_s_at	FADS1	Fatty acid desaturation	1.65
208847_s_at	ADH5	Ethanol oxidation	1.56
205353_s_at	PBP	Lipid binding	1.39
225908_at	LOC285148	Lipid metabolism	1.39
209608_s_at	ACAT2	Lipid metabolism	1.31
Protein biosynthesis/metabolism			
229357_at	ADAMTS5	Proteolysis and peptidolysis	3.43
202620_s_at	PLOD2	Protein metabolism	2.83
202381_at	ADAM9	Proteolysis and peptidolysis	1.99
219117_s_at	FKBP11	Protein folding	1.91
204017_at	KDELR3	Protein transport	1.87
224002_s_at	FKBP7	Protein folding	1.79
209004_s_at	FBXL5	Protein ubiquitination	1.75
200839_s_at	CTSB	Proteolysis and peptidolysis	1.67
220750_s_at	LEPRE1	Protein metabolism	1.65
201487_at	CTSC	Proteolysis and peptidolysis	1.64
205133_s_at	HSPE1	Protein folding	1.59
203781_at	MRPL33	Protein biosynthesis	1.55
212433_x_at	RPS2	Protein biosynthesis	1.54
222997_s_at	MRPS21	Protein biosynthesis	1.49
224930_x_at	RPL7A	Ribosome biogenesis and assembly	1.48
208856_x_at	RPLP0	Protein biosynthesis	1.47
218654_s_at	MRPS33	Protein biosynthesis	1.45
207585_s_at	RPL36AL	Protein biosynthesis	1.44
200095_x_at	RPS10	Protein biosynthesis	1.41
200095_x_at	RPS10	Protein biosynthesis	1.41
213687_s_at	RPL35A	Protein biosynthesis	1.40
212933_x_at	RPL13	Protein biosynthesis	1.39
226749_at	MRPS9	Protein biosynthesis	1.36
200088_x_at	RPL12	Protein biosynthesis	1.36
217740_x_at	RPL7A	Protein biosynthesis	1.34
200963_x_at	RPL31	Protein biosynthesis	1.33
200034_s_at	RPL6	Structural constituent of ribosome	1.29
200781_s_at	RPS15A	Structural constituent of ribosome	1.29
234875_at	RPL7AP3	Ribosome biogenesis and assembly	1.28
209467_s_at	MKNK1	Regulation of translation	1.27
222229_x_at	RPL26	Protein biosynthesis	1.27
Signaling			
204602_at	DKK1	Wnt receptor signaling pathway	3.18
205302_at	IGFBP1	Signal transduction	3.05
210986_s_at	TPM1	Negative regulation of Ras protein signal transduction	2.27
202404_s_at	COL1A2	Protein tyrosine kinase signaling pathway	2.23
228141_at	NUDT4	Intracellular signaling cascade	2.14
202037_s_at	SFRP1	Wnt receptor signaling pathway	2.11
201667_at	GJA1	Positive regulation of I-κB kinase/NF-κB cascade	2.07
212724_at	RND3	Small GTPase mediated signal transduction	1.99
218236_s_at	PRKD3	Intracellular signaling cascade	1.95
200093_s_at	HINT1	Signal transduction	1.77

TABLE 2. *Continued*

Identifier	Symbol	Gene ontogeny (biological process, molecular function)[a]	Fold Δ
201923_at	PRDX4	I-κB phosphorylation	1.75
213923_at	RAP2B	Small GTPase mediated signal transduction	1.75
228109_at	RASGRF2	Small GTPase mediated signal transduction	1.74
204595_s_at	STC1	Cell-cell signaling	1.72
203434_s_at	MME	Cell-cell signaling	1.67
204319_s_at	RGS10	Negative regulation of signal transduction	1.64
227250_at	KREMEN1	Wnt receptor signaling pathway	1.61
217764_s_at	RAB31	Small GTPase mediated signal transduction	1.61
226651_at	HOMER1	Phospholipase C activating pathway	1.59
Transcription			
201417_at	SOX4	Transcription	2.89
212762_s_at	TCF7L2	Transcription	2.73
207558_s_at	PITX2	Regulation of transcription, DNA-dependent	2.39
209357_at	CITED2	Regulation of transcription from RNA polymerase II promoter	2.20
213139_at	SNAI2	Transcription	2.06
201200_at	CREG1	Regulation of transcription from RNA polymerase II promoter	1.91
210002_at	GATA6	Transcription	1.77
201231_s_at	ENO1	Transcription	1.64
213357_at	GTF2H5	Regulation of transcription; DNA repair	1.61
203316_s_at	SNRPE	Spliceosome assembly	1.55
202306_at	POLR2G	Transcription	1.28
225533_at	PHF19	Regulation of transcription, DNA dependent	1.27
Transport			
201243_s_at	ATP1B1	Transport	2.13
232458_at	COL3A1	Phosphate transport	2.06
217801_at	ATP5E	Proton transport	1.75
219090_at	SLC24A3	Ion transport	1.69
209884_s_at	SLC4A7	Anion transport	1.56
227647_at	KCNE3	Ion transport	1.44
201754_at	COX6C	Electron transport	1.35
Other			
209335_at	DCN	Organogenesis	3.05
226517_at	BCAT1	Cell proliferation	2.48
208949_s_at	LGALS3	Sugar binding	2.10
204971_at	CSTA	Cysteine protease inhibitor activity	2.06
203304_at	BAMBI	Integral to membrane	2.03
39729_at	PRDX2	Response to oxidative stress	2.00
204222_s_at	GLIPR1	Extracellular region	1.92
226853_at	BMP2K	Protein amino acid phosphorylation	1.74
209377_s_at	HMGN3	Thyroid hormone receptor binding	1.72
221675_s_at	CHPT1	Platelet activating factor biosynthesis	1.72
223092_at	ANKH	Locomotory behavior	1.59
208690_s_at	PDLIM1	Response to oxidative stress	1.69
201842_s_at	EFEMP1	Visual perception	1.68
202429_s_at	PPP3CA	Protein amino acid dephosphorylation	1.67
217892_s_at	EPLIN	Metal ion binding	1.60
212282_at	MAC30	Regulation of cell growth	1.59
207543_s_at	P4HA1	Oxidoreductase activity	1.56
221556_at	CDC14B	Protein amino acid dephosphorylation	1.54
225272_at	SAT2	Acyltransferase activity	1.54
201470_at	GSTO1	Metabolism	1.51
200872_at	S100A10	Calcium ion binding	1.43
203152_at	MRPL40	Morphogenesis	1.42
218493_at	C16orf33	Nuclear mRNA splicing, via spliceosome	1.39
204839_at	POP5	tRNA processing	1.38
205849_s_at	UQCRB	Aerobic respiration	1.32
Unknown			
236034_at	MCPH1		4.69
223395_at	ABI3BP		4.29
226834_at	ASAM		2.69
218162_at	OLFML3		2.22
219014_at	PLAC8		2.20
223623_at	ECRG4		2.07
212686_at	PPM1H		2.04
226763_at	SESTD1		1.95
230263_s_at	DOCK5		1.93
222396_at	HN1		1.89
219191_s_at	BIN2		1.88

TABLE 2. *Continued*

Identifier	Symbol	Gene ontogeny (biological process, molecular function)[a]	Fold Δ
221210_s_at	NPL		1.85
213911_s_at	H2AFZ		1.77
228109_at	RASGRF2		1.74
226853_at	BMP2K		1.74
227291_s_at	BOLA3		1.64
201201_at	CSTB		1.61
223136_at	AIG1		1.61
209014_at	MAGED1		1.57
211628_x_at	FTHP1		1.53
203405_at	DSCR2		1.53
218477_at	TMEM14A		1.53
238587_at	STS-1		1.52
210825_s_at	PBP		1.51
218140_x_at	SRPRB		1.51
224707_at	ORF1-FL49		1.49
215785_s_at	CYFIP2		1.48
224995_at	SPIRE1		1.47
226336_at	PPIA		1.46
223711_s_at	THY28		1.44
37408_at	MRC2		1.42
207243_s_at	CALM2		1.40
223086_x_at	MRPL51		1.39
202391_at	BASP1		1.33
228882_at	TUB		1.29
225533_at	PHF19		1.27
Hypothetical proteins			
219791_s_at	NBLA00301		3.56
226464_at	MGC33365		2.79
221802_s_at	KIAA1598		2.00
227280_s_at	FLJ40432		1.75
225380_at	LOC91461		1.68
221791_s_at	HSPC016		1.59
223095_at	MARVELD1		1.51
227466_at	LOC285550		1.44
225908_at	LOC285148		1.39
228249_at	LOC119710		1.27
ORF			
212055_at	C18orf10		1.68
219065_s_at	C2orf4		1.66
224867_at	C1orf151		1.53
218597_s_at	C10orf70		1.52
224879_at	C9orf123		1.44
212115_at	C16orf34		1.36
222785_x_at	C11orf1		1.33
Nonannotated			
232090_at	NA		1.93
229004_at	NA		1.87
228479_at	NA		1.87
238617_at	NA		1.87
229004_at	NA		1.87
212195_at	NA		1.65
223366_at	NA		1.48
229615_at	NA		1.22

ORF, Open reading frame.
[a] Obtained from www.genetools.microarray.ntnu.no as of March 2006.

Confirmation of the microarray results

To further validate the microarray data, we used two approaches: quantitative PCR (Q-PCR) to assess relative mRNA levels and immunolocalization to confirm differential expression at the protein level. With regard to Q-PCR, our analysis focused primarily on the genes that exhibited the greatest fold change and those that encoded hypothetical proteins with potentially novel functions. The sequences of the primer/probe sets are shown as supplemental data (supplemental Table 2). The 14 genes that we subjected to Q-PCR analyses all showed the expected expression patterns (Fig. 4). Six were up-regulated: CRH, hypothetical protein LOC284561, mucin 15 , trophoblast-derived noncoding RNA, hypothetical protein FLJ11292, and platelet/endothelial cell adhesion molecule-1 (Fig. 4A). Eight were down-regulated: MCPH1, target of Nesh-SH3, chemokine ligand 14, hypothetical protein FLJ11539, phospholipase A2, group VII, transcription factor-like 2, adipocyte-specific adhesion molecule, and vascular

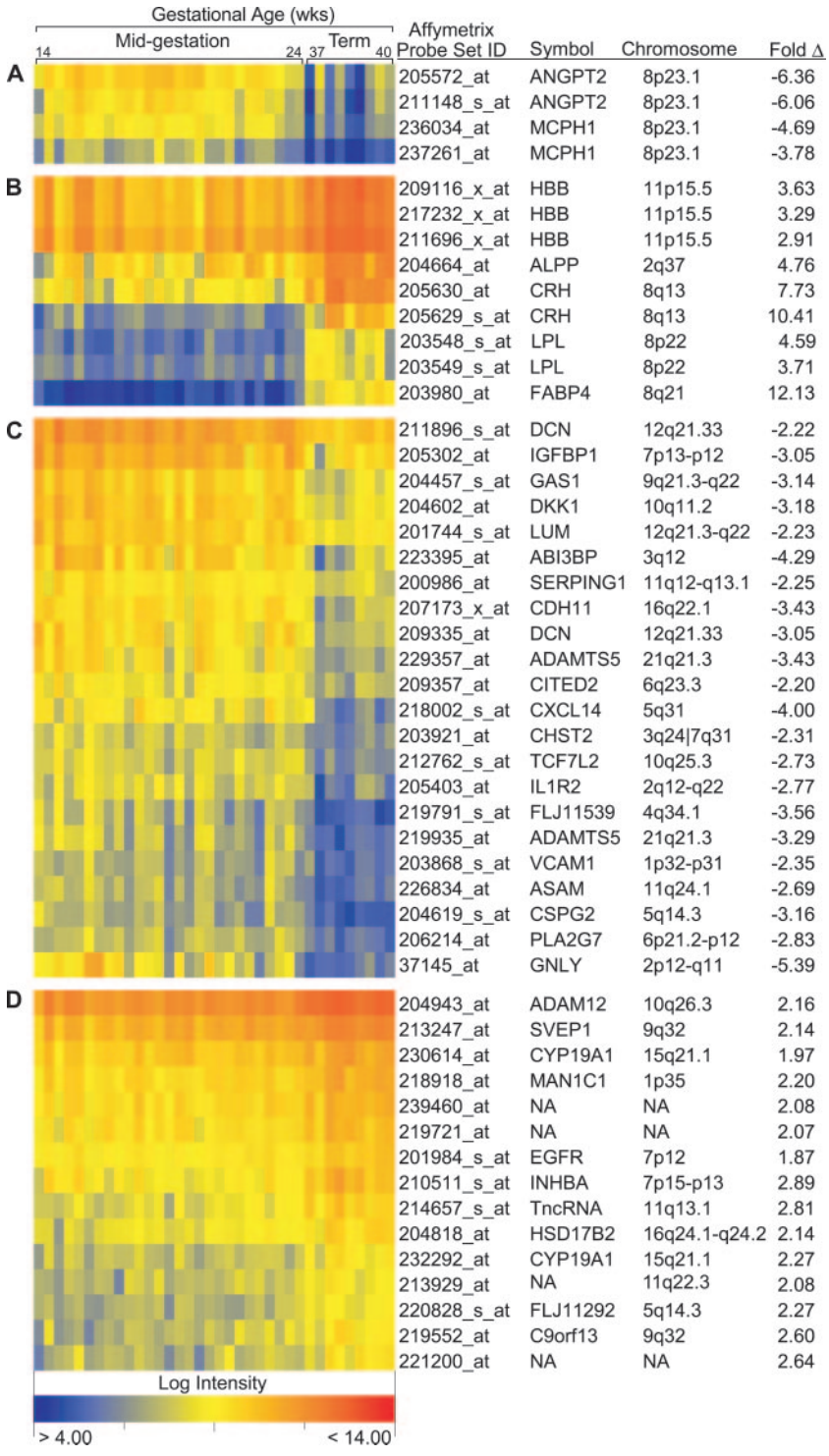

FIG. 3. Selected K-means clusters of differentially expressed genes that are coexpressed. Differentially expressed probe sets were clustered into 11 groups using K-means (Euclidean). Clusters A, B, C, and D are presented as heat maps of the normalized log intensity data, which allows visual assessment of the signal intensity and the degree of change over gestation. Arrays (*columns*) are arranged from left to right, ordered by increasing gestational age. Each probe set is annotated with the probe set ID, gene symbol, chromosomal location, and fold change. The seven additional clusters that were generated are included as supplemental data (supplemental Fig. 3).

cell adhesion molecule 1 (Fig. 4B). Additionally, the Q-PCR data and log intensity values for each basal plate specimen showed a high degree of cross-correlation (Fig. 4, A and B).

With regard to the immunolocalization experiments, we focused on LPL, one of the lipid metabolizing enzymes that were highly up-regulated (3.7-fold) at the mRNA level over gestation. The staining pattern of LPL, which was primarily cytoplasmic, changed with advancing gestational age. Specifically, at 16 wk, the vast majority of cells in the basal plate region, including CK-positive CTBs within the uterine wall, failed to react with anti-LPL (Fig. 5A, b and c). At 23 wk, a slightly higher level of immunoreactivity was detected, pri-

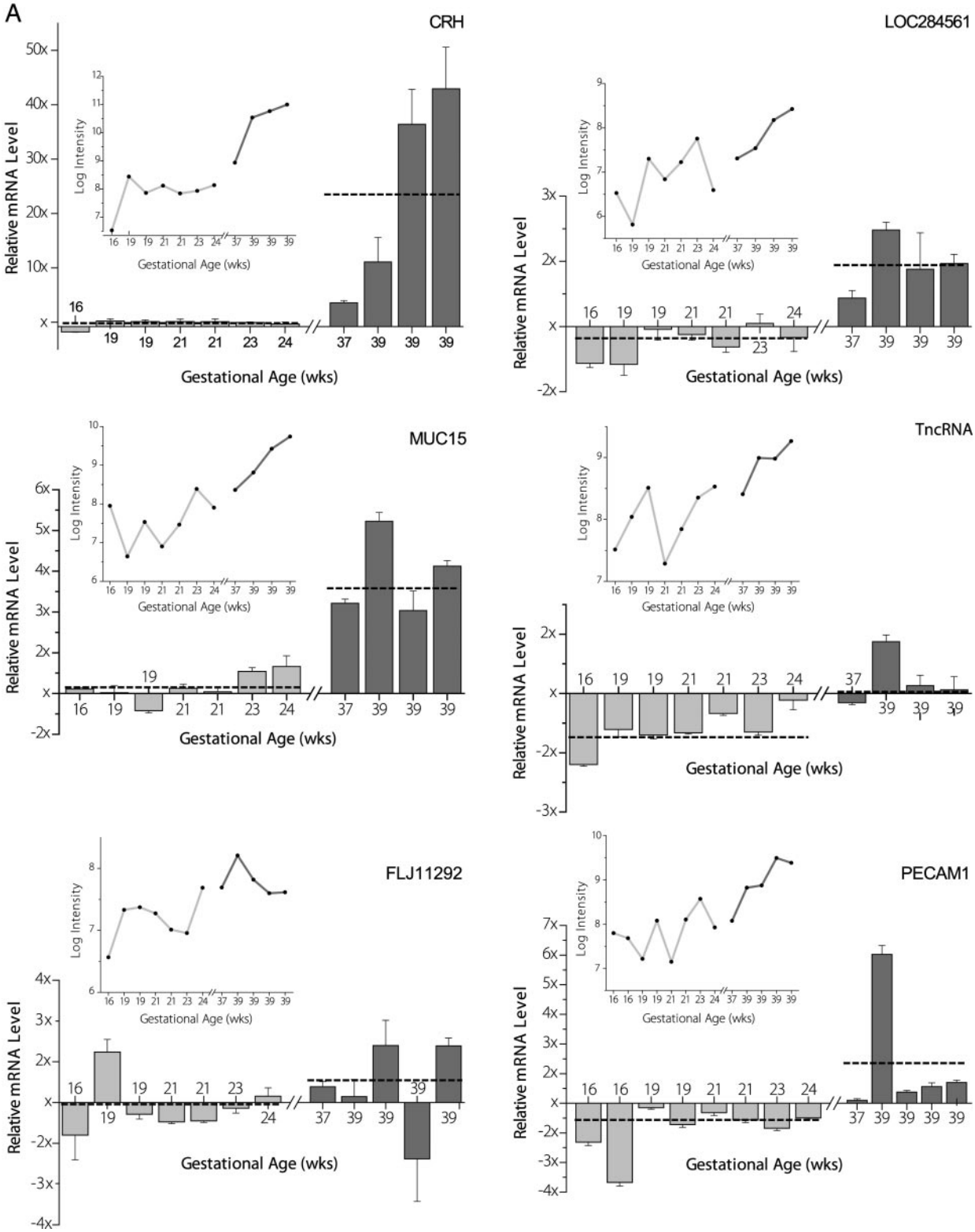

FIG. 4. Q-PCR confirmation of a subset of differentially expressed genes. Samples of total RNA isolated from basal plate biopsy specimens that were obtained at midgestation (14–24 wk; n = 8 or 9) or term (37–40 wk; n = 4 or 5) were analyzed using TaqMan primer/probe sets. A, Q-PCR data for transcripts up-regulated at term: CRH ($P = 0.0003$), hypothetical protein LOC284561 ($P = 0.0006$), mucin 15 (MUC15; $P = 0.00002$), trophoblast-derived noncoding RNA (TncRNA; $P = 0.01$), hypothetical protein FLJ11292 ($P = 0.04$), and platelet/endothelial cell adhesion molecule-1 (PECAM1; $P = 0.03$). Relative RNA levels were normalized to 18S values and then divided by a calibrator, in this case a 14-wk sample. Each *bar* represents the mean ± SD of triplicate determinations (midgestation, *light gray*; term, *dark gray*). *Dashed lines* are the mean values for the midgestation or term samples. Significance was determined by using Student's *t* test ($P < 0.05$). For comparison, the *insets* show the corresponding microarray log intensity data for the same samples ($\log_2$).

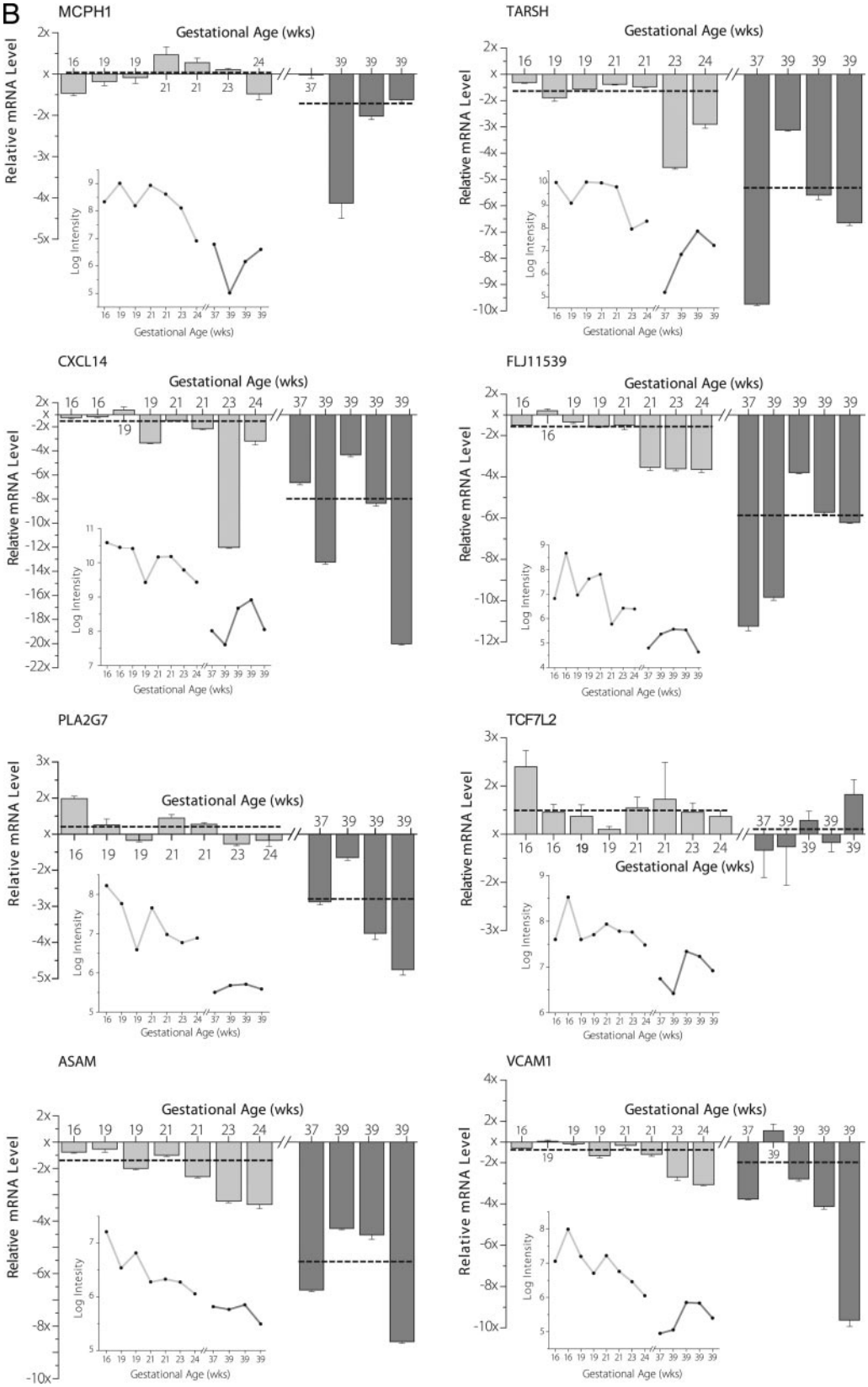

FIG. 4. *Continued.* B, Q-PCR data for transcripts down-regulated at term: MCPH1 ($P = 0.054$), target of Nesh-SH3 (TARSH; $P = 0.008$), chemokine (C-X-C motif) ligand 14 (CXCL14; $P = 0.02$), hypothetical protein FLJ11539 ($P = 0.008$), phospholipase A2, group VII (PLA2G7; $P = 0.002$), transcription factor-like 2 (TCF7L2; $P = 0.12$), adipocyte-specific adhesion molecule (ASAM; $P = 0.01$), and vascular cell adhesion molecule 1 (VCAM1; $P = 0.34$).

marily in association with CTBs; intense staining was occasionally observed (Fig. 5A, e and f). In contrast, many CTBs exhibited strong immunoreactivity at 39 wk (Fig. 5A, h and i), and minimal staining was detected in association with the decidua.

We also used an immunolocalization approach to validate up-regulation of FABP4 expression at term. In accord with the microarray data, faint immunoreactivity was detected in association with cells of the basal plate during the second trimester. Maternal cells (CK negative) expressed FABP4 in the cytoplasmic compartment (Fig. 5B, c), although occasional nuclear staining was also observed in some of the earlier gestation samples (data not shown). Fetal cells (CK-positive trophoblasts) showed essentially no FABP4 staining. In contrast, strong FABP4 immunoreactivity was detected in association with cells of the basal plate at term. In general, the fetal cells had intense nuclear and minimal cytoplasmic staining. Maternal cells had a similar staining pattern, but at much lower levels (Fig. 5B, f).

Protein modeling to gain insight into possible functions of the nonannotated differentially expressed genes

Given the large number of hypothetical proteins and nonannotated sequences among the differentially expressed genes, we used modeling to gain insight into their potential functions. Of the 78 hypothetical proteins or nonannotated sequences encoded by the differentially expressed genes that

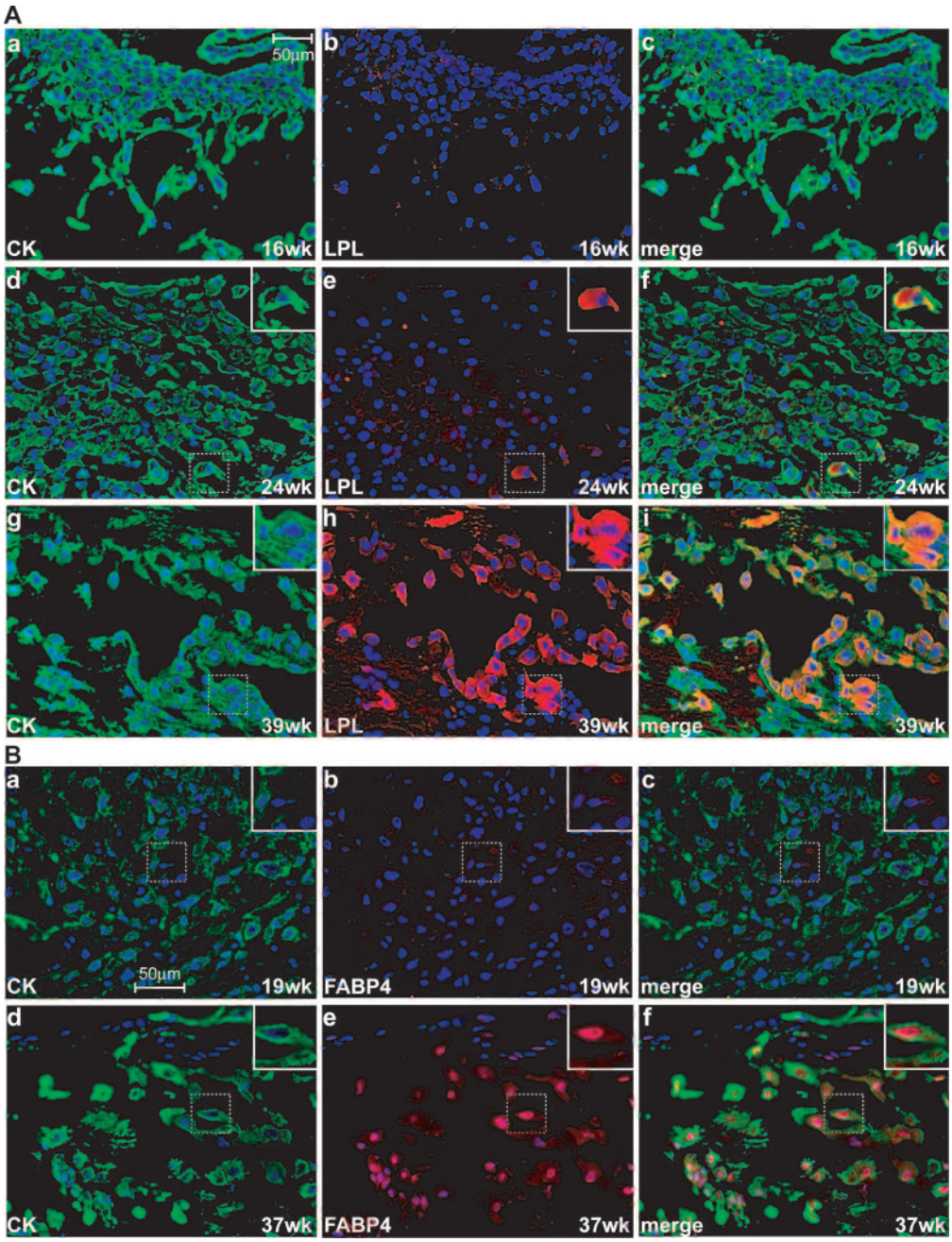

FIG. 5. Invasive CTBs up-regulate expression of LPL and FABP4 at term. A, Tissue sections of basal plate biopsy specimens from 16-wk (a–c), 23-wk (d–f), and 39-wk (g–i) placentas were double stained with anti-CK (1:50; a, d, and g) to identify CTBs and an anti-LPL antibody, 5D2 (1:100; b, e, and h; the kind gift of J. D. Brunzell, University of Washington). Binding was detected with the appropriate species-specific secondary antibodies. Nuclei were labeled with Hoechst (1:1000; *blue*). Merging of the *green* (CK) and *red* (LPL) images showed that CTBs stained for LPL, and expression increased dramatically with advancing gestational age (c, f, and i). Each *inset* is a ×63 magnification of the region contained within the *white dashed lines* (d–i). Photos are representative of the basal plate staining at 16 wk (n = 3), 23–24 wk (n = 5), and 37–40 wk (n = 4). B, Expression of FABP4, which is localized to the nuclei of human basal plate CTBs, increased expression at term. Human basal plate biopsy specimens from 19-wk (a–c) or 37-wk (d–f) placentas were stained with anti-CK (1:50) to identify the invasive CTBs (a and d) and Hoechst (1:1000) to identify nuclei. Sections were costained with anti-FABP4 antibody (1:1000; b and e). Strong FABP4 immunoreactivity was detected in association with cells of the basal plate at term, compared with the second trimester (compare b and e). CK-positive CTBs stained primarily in a nuclear pattern, whereas staining in maternal cells was largely in the cytoplasmic compartment (c and f). Photos are representative of the basal plate staining at midgestation (15–24 wk; n = 11) and term (n = 3).

were evaluated, 31 were reliably annotated for potential functions. These results are shown in Table 3. Subsets of potential functions included myosin related molecules, enzymes, and ribosomal-like proteins. The complete analysis with links to the MODBASE models is provided as supplemental data (supplemental Table 4).

Discussion

We performed a global analysis of gene expression profiles at the human maternal-fetal interface between midgestation (14–24 wk) and term (37–40 wk). The 418 differentially expressed genes included molecules with well-characterized expression patterns, specifically up-regulation of CRH, and the inhibin-βA subunit and down-regulation of C-X-C chemokine ligand 14 and angiopoietin-2, which served as positive controls. The analysis also revealed a number of novel observations, such as the large proportion of nonannotated or hypothetical proteins. Independent analyses of the expression patterns of 16 of the most highly regulated genes gave the predicted results, suggesting the validity of the data set as a whole. The differentially expressed genes encompassed numerous biological processes, including angiogenesis, cell motility, extracellular matrix modulation, gene transcription, signal transduction, immune response, protein biosynthesis, and lipid metabolism. The significance of a portion of these data are discussed in greater detail below. K-means cluster analysis showed that some genes were tightly coexpressed, suggesting the possibility of common regulatory mechanisms. Pathway analysis demonstrated significant alterations in several metabolic and signaling processes. Most notably, a number of differentially expressed genes were associated with folate biosynthesis, *N*-glycan biosynthesis, and Wnt-β-catenin signaling. Modeling of the hypothetical proteins and nonannotated sequences suggested possible functions for a subset of these putative molecules. Together, these data provide new insights into the dynamics

TABLE 3. Functional annotation determined from protein modeling

ProbeSet ID	e Value	Annotation method	Potential protein functional annotation
239365_at[a]	0	Homology	Scinderin (SCIN)
232292_at[a]	1.00E-120	Homology	Cytochrome P450 19A1(EC 1.14.14.1) (aromatase; estrogen synthetase)
225316_at	7.00E-05	Homology	Lactose permease (PFAM); hypothetical protein FLJ35904
225499_at	1.00E-82	Homology	KIAA1272 protein (fragment); GTPase-activating protein
230277_at	2.00E-82	Homology	Zinc finger protein 655 (ZNF655); VIK protein (pyruvate-ferredoxin oxidoreductase); Vav-interacting Kruppel-like protein
232852_at[a]	8.00E-16	Homology	LIM domain-binding protein 2 (LDB2); carboxyl-terminal LIM domain-binding protein 1 (CLIM-1)
211972_x_at[a]	2.60E-05	Homology	60s acidic ribosomal protein p0 (l10e)
229004_at[a]	1.00E-50	Homology	ADAMTS-15 precursor (ec 3.4.24.-) (a disintegrin and metalloproteinase with thrombospondin motifs 15)
225987_at[a]	2.00E-32	Homology	STEAP4 protein
220187_at[a]	2.00E-32	Homology	STEAP4 protein
212327_at[a]	3.00E-22	Homology	KIAA1102 protein (fragment) (calponin α:calponin homology domain)
228568_at[a]	3.00E-09	Homology	Myosin II heavy chain fused to α-actinin 3: myosin II heavy chain, motor domain
220003_at	7.00E-06	Homology	Tropomyosin
226599_at[a]	4.00E-83	Homology	KIAA1727 protein (diaphanous protein homolog)
229144_at[a]	6.00E-10	Homology	KIAA1026 protein (fragment) myosin II heavy chain fused to α-actinin 3: II heavy chain,motordomain
229910_at[a]	5.00E-18	Homology	FLJ00138 protein (fragment) 3-kinase regulatory α3-subunit)
214076_at	2.00E-38	Homology	Precursor form of glucose-fructose 3 oxidoreductase
221028_s_at	2.00E-38	Homology	Precursor form of glucose-fructose 3 oxidoreductase
219431_at[a]	7.00E-44	Homology	GRAF2
228233_at[a]	4.00E-48	Homology	FREM1 protein
209191_at[a]	1.00E-162	Homology	Tubulin, β6
227280_s_at	3.00E-08	Homology	Cyclin a
221802_s_at	2.00E-08	Homology	Myosin II heavy chain fused to α-actinin 3: myosin II heavy chain, motor domain + fibrinogen
237261_at[a]	2.00E-83	Homology	Angiopoietin-2 precursor (ANG2)
225467_s_at[a]	4.00E+00	Homology	Shikimate 5′-dehydrogenase
229055_at[a]	2.00E-17	Homology	Ovarian cancer G-protein-coupled receptor 1
224915_x_at[a]	9.00E-04	Threading	Similar to glycosylated five-domain human-glycoprotein I purified from blood plasma
224930_x_at[a]	1.00E-25	Homology	Ribosomal protein l7a
232090_at[a]	2.00E-58	Homology	Dynamin (pleckstrin homology domain)
227466_at	4.00E-05	Threading	Similar to hermes DNA transposase
236034_at[a]	2.00E-83	Homology	Angiopoietin-2

[a] Affymetrix with new annotations posted April 2006 (see supplemental Table 4 for comparison).

of gene expression at the human maternal-fetal interface during pregnancy and numerous directions for additional functional analyses.

To our knowledge, this is the first application of a microarray approach for profiling the gene expression patterns over gestation of the conjoined areas of the human placenta and decidua that compose the maternal-fetal interface. Given the revised estimate that the human genome contains 29,000–36,000 protein-encoding genes (37), our analysis of 39,000 transcripts generated a comprehensive data set. We note that other investigators have used microarray technologies to evaluate gene expression patterns during human trophoblast or placental development. Cheng *et al.* (11) used a cDNA platform with 9600 cloned sequences to separately evaluate the gene expression profiles of first-trimester decidua and chorionic villi. In their analysis, the maternal-fetal interface was deliberately excluded. Recently Wyatt *et al.* (38) compared gene expression patterns of samples taken from the medial and lateral portions of the placenta. In many instances, no spatial variations were noted, but in a few cases, up to a 3-fold difference was observed. Although that paper was published after the samples for our study had been collected, we took this potentially confounding factor into account by pooling samples from both locations. Most recently Sood *et al.* (39) reported the gene expression profiles of different anatomical locations of human placentas that were obtained after normal term deliveries.

In this study, our goal was to begin to analyze the molecular components of the dialogue that takes place between maternal and fetal cells in the human basal plate region over gestation. In interpreting the microarray data obtained from analysis of this complex tissue, we were cognizant of the fact that differential gene expression could reflect changes that involve one or multiple cell types, with alterations in the cellular composition of the basal plate region yet another possibility. Further investigation of the expression patterns and biological functions of the up- and down-regulated molecules will shed additional light on this issue. Another potential confounder could be maternal blood contamination. The maternal-fetal interface is richly vascularized, and blood flow to this region increases at term. Furthermore, it is impossible to completely remove blood cells from this tissue, even by multiple washes in large volumes of PBS, the procedure we used. Therefore, the expression levels of hemoglobin-β, a transcript that is highly expressed in red blood cells, were evaluated in relationship to the expression patterns of the differentially expressed genes. This analysis showed that only hemoglobin-δ expression correlated tightly with that of hemoglobin-β (Pearson's coefficient $r^2 = 0.92$), followed by Kruppel-like factor 2 ($r^2 = 0.757$), which was below the level of significance. Therefore, these results suggest that none of the expression patterns of the other differentially expressed genes can be solely explained by varying amounts of blood contamination. Finally, drug exposure could also be a possible confounder because we did not have access to the clinical data regarding the type of sedation that was used in each case. In general, the midgestation procedures were performed under conscious sedation (fentenyl and versed), and patients who underwent cesarean sections had regional anesthesia (epidural or spinal).

Because the basal plate region is comprised of a mixture of maternal and fetal cells, we also determined whether changes in the proportion of cytotrophoblasts could account for any of the differentially expressed genes. To address this possibility, we exploited the fact that approximately 50% of the placentas were from pregnancies in which the fetus was male. We thus estimated the contribution of fetal cells by examining the expression patterns of two Y-linked genes, ribosomal protein S4–1 and (DEAD) box polypeptide 3. Analysis of the data showed that the log intensity values of these probe sets had less variability than those of the differentially expressed genes. Furthermore, there was no significant correlation between the expression patterns of these transcripts and genes that were either up- or down-regulated over gestation (Pearson correlation coefficients < 0.8). Additionally none of the differentially expressed genes showed significant correlations with cytokeratin-7, which is specifically expressed by all the trophoblast populations in this region (Pearson > 0.08). Together, these data suggest that the observed changes in gene expression were unlikely to be attributable to variable contributions of fetal cells to the basal plate samples we analyzed.

With regard to specific categories of the differentially expressed genes, we were particularly interested in those that we had not expected to show dramatic patterns of regulation, *e.g.* molecules that play a role in lipid metabolism. As a result, we included a number of these gene products in the validation studies. Immunolocalization of LPL and FABP4 illustrated the fact that the differentially expressed genes that were identified in the microarray analysis can reflect changes that occur in either a single cell type or both maternal and fetal cells. Specifically, our analysis showed that invasive CTBs dramatically up-regulated expression of cytoplasmic LPL levels at term with minimal expression noted in maternal cells. This pattern of regulation is in contrast to maternal plasma LPL levels, which decrease during human pregnancy (40). It is possible that the increase of CTB LPL expression at term occurs in response to an increased demand for fatty lipid precursors that are used in the synthesis of prostaglandins required for labor. This theory is supported by the analysis of the LPL immunoreactivity that is associated with the cells that compose the human fetal membranes at term (*i.e.* the location of known prostaglandin production for parturition). Specifically, anti-LPL localized to the basolateral surface of amniotic epithelia, the chorionic CTB layer exhibited plasma membrane immunoreactivity, and the extracellular compartment stained as well (41). It is interesting to note that invasive CTBs and cells of the amnion/chorion appear to have different subcellular patterns of LPL distribution. In this regard, the fetal membranes studied by Huter *et al.* (41) were obtained after vaginal delivery, whereas our samples were obtained from patients who did not experience labor. Together, these findings suggest that LPL might be stored within the cell before initiation of parturition, subsequently localizing to the plasma membrane and extracellular compartment during the delivery process.

The expression of FABP4, or adipocyte P2, which plays a role in lipid signal transduction, also increased dramatically

at term predominantly in the invasive CTBs; decidual cell expression was detected from midgestation onward. This molecule, which is highly expressed in adipose tissue, serves as a marker of adipocyte maturation (42). Like other FABPs, its functions include fatty acid uptake and intracellular shuttling (43). Consistent with this role, FABP4 physically interacts with the hormone-sensitive lipase of adipose tissue, binding a fatty acid product, thereby facilitating lipolysis (44) and intracellular delivery of ligands to regulatory proteins. Indeed, FABP4 specifically provides lipid ligands to the nuclear receptor peroxisome proliferative activated receptor-γ, which in turn regulates gene transcription (45). To our knowledge, this is the first report of FABP4 expression in the human basal plate. Of note is the fact that FABP4, LPL, and CRH (cluster B) had very similar expression patterns, with r^2 values of 0.84 to 0.85. The coexpression of these molecules in the basal plate region suggests that enhanced availability of fatty acids may be part of the molecular preparation for parturition. The coregulation of these molecules also raises the possibility that CRH may govern LPL and FABP4 expression. In this regard, there is a recent report that CRH influences the functions of other lipases (46). Alternatively, the coexpression of all three molecules might be governed by a higher-order mechanism, the basis of which could provide important new clues to the signals that trigger labor.

Examination of the highly regulated immune molecules highlighted the possibility that changes in gene expression could reflect alterations in the cellular composition of the basal plate. The expression of granulysin, which localizes to the cytolytic granules of T cells, natural killer (NK) cells (47), and certain dendritic cells (48), is down-regulated at term. We speculate that the decreased expression we observed reflects the known parallel decrease in the number of T and NK cells at the maternal-fetal interface at term (49). The down-regulation of the expression of Ly96, another NK cell-specific molecule, provides further support for this concept. Although the mechanisms that lead to the eventual disappearance of decidual leukocytes from the maternal-fetal interface are not known, the decrease in expression noted for the chemotactic molecules, such as chemokine-like factor superfamily 6 and secreted phosphoprotein 1 (Table 2), could be a related phenomenon.

Our group has also been interested in the functions of the myriad of angiogenic factors that are produced at the maternal-fetal interface (3, 50). Consistent with our previously published work, we found that the down-regulated genes included ANGPT-2 (51). This microarray analysis also revealed a striking co-down-regulation at term of ANGPT-2 and MCPH1. MCPH1 controls brain size in humans by regulating the proliferative and hence differentiative capacity of neuroblasts, ultimately exerting its affects through cell cycle regulators such as checkpoint kinase 1 and breast cancer 1 (38, 52). MCPH1 was previously reported to be expressed by (fetal) brain, liver and kidney. Thus, it will be interesting to determine which cell type(s) at the maternal-fetal interface expresses this molecule. Additional analysis of the ANGPT-2 and MCPH1 genes revealed they are transcribed from opposite strands of the same region (chromosome 8p23.1). Their tight co-expression suggests that transcription from this area could be silenced at term, perhaps by local chromatin modifications or the recruitment of inhibitory protein complexes to the same promoter element. It will be interesting to determine whether the pattern of coexpression of ANGPT-2 and MCPH1 occurs in other tissues or is placental specific. Finally, there is evidence that strong genetic selection has been exerted on MCPH1 during recent human evolution (53). Whereas the most obvious selection pressure may be on brain size, another interesting possibility is that the placenta is coevolving.

In summary, the maternal-fetal interface is a remarkable chimeric tissue that holds the answers to many interesting biological questions regarding invasive behavior, vasculogenesis/angiogenesis and immunotolerance. Our study provides a global analysis of the expression patterns of genes that are involved in these and other processes. The fact that molecules with known expression patterns were correctly regulated bolsters our confidence in the novel data we obtained. Finally, the results of this study provide reference data sets of gene expression profiles against which changes that occur in a variety of pregnancy complications can be measured. For example, impaired CTB invasion has been associated with recurrent miscarriages (54, 55), preeclampsia (56), intrauterine growth restriction (56), and a subset of preterm labor cases (57). Now we are in a position to differentiate changes in gene expression that occur in these conditions from those that are attributable to advancing gestational age.

Acknowledgments

We thank Ms. Jean Perry, the study research nurse coordinator, who assisted in tissue collection, as did the nurses, residents, and faculty at San Francisco General Hospital Women's Options Center and the UCSF Birth Center. Dr. Chris Barker, Dr. Chandi Griffin, and Ms. Jennifer Gregg, members of the UCSF Gladstone (National Heart, Lung, and Blood Institute) Shared Microarray Facility, contributed invaluable technical and intellectual expertise. We also thank Drs. David Erle and Michael Salazar, members of the Sandler Genomics Core Facility, for helpful discussions and assistance with data deposition. We are grateful to Mr. Evan Messenger and Dr. Kathy Ivanetich, UCSF Biomolecular Research Center, for technical assistance in performing the Q-PCR experiments. We thank Dr. John Brunzell (University of Washington) for the kind gift of the LPL-specific antibody that was used in the immunolocalization studies. Finally, we are grateful to Ms. Mary McKenney and Dr. Leonard Dragone for critical review of the manuscript.

Received May 19, 2006. Accepted December 4, 2006.

Address all correspondence and requests for reprints to: Virginia D. Winn, M.D., Ph.D., University of Colorado Health Sciences Center, Reproductive Science, Mail Stop 8309, 12800 East 19th Avenue, P.O. Box 6511, Aurora, Colorado 80045. E-mail: virginia.winn@uchsc.edu.

This work was supported by National Institutes of Health Grants R01 HL 64597 (to S.J.F.), R21 AI53782 (to L.P.), DK 053189 (to D.A.B.), 5-MO1-RR 00083 (General Clinical Research Center, San Francisco General Hospital), and HL 072301 (University of California, San Francisco, National Heart, Lung, and Blood Institute Shared Microarray Facility). V.D.W. is a March of Dimes Reproductive Scientists Development Program scholar (National Institute of Child Health and Human Development 5K12HD00849) and an American Board of Obstetrics and Gynecology/American Association of Obstetricians and Gynecologists Foundation scholar.

Author Disclosure Summary: V.D.W., R.H.-K., A.C.P., Y.J.Y., M.S.M., M.G., K.-T.V.F., S.M., L.P., A.S., and S.J.F. have nothing to declare. D.A.B. has received lecture fees from Merck and Pfizer.

References

1. **Damsky CH, Librach C, Lim KH, Fitzgerald ML, McMaster MT, Janatpour M, Zhou Y, Logan SK, Fisher SJ** 1994 Integrin switching regulates normal trophoblast invasion. Development 120:3657–3666
2. **Zhou Y, Fisher SJ, Janatpour M, Genbacev O, Dejana E, Wheelock M, Damsky CH** 1997 Human cytotrophoblasts adopt a vascular phenotype as they differentiate. A strategy for successful endovascular invasion? J Clin Invest 99:2139–2151
3. **Red-Horse K, Zhou Y, Genbacev O, Prakobphol A, Foulk R, McMaster M, Fisher SJ** 2004 Trophoblast differentiation during embryo implantation and formation of the maternal-fetal interface. J Clin Invest 114:744–754
4. **Clark DE, Smith SK, Licence D, Evans AL, Charnock-Jones DS** 1998 Comparison of expression patterns for placenta growth factor, vascular endothelial growth factor (VEGF), VEGF-B and VEGF-C in the human placenta throughout gestation. J Endocrinol 159:459–467
5. **Zhou Y, McMaster M, Woo K, Janatpour M, Perry J, Karpanen T, Alitalo K, Damsky C, Fisher SJ** 2002 Vascular endothelial growth factor ligands and receptors that regulate human cytotrophoblast survival are dysregulated in severe preeclampsia and hemolysis, elevated liver enzymes, and low platelets syndrome. Am J Pathol 160:1405–1423
6. **Staun-Ram E, Goldman S, Gabarin D, Shalev E** 2004 Expression and importance of matrix metalloproteinase 2 and 9 (MMP-2 and -9) in human trophoblast invasion. Reprod Biol Endocrinol 2:59
7. **Librach CL, Feigenbaum SL, Bass KE, Cui TY, Verastas N, Sadovsky Y, Quigley JP, French DL, Fisher SJ** 1994 Interleukin-1β regulates human cytotrophoblast metalloproteinase activity and invasion *in vitro*. J Biol Chem 269:17125–17131
8. **McMaster MT, Librach CL, Zhou Y, Lim KH, Janatpour MJ, DeMars R, Kovats S, Damsky C, Fisher SJ** 1995 Human placental HLA-G expression is restricted to differentiated cytotrophoblasts. J Immunol 154:3771–3778
9. **Mattsson R** 1998 The non-expression of MHC class II in trophoblast cells. Am J Reprod Immunol 40:383–384
10. **Aronow BJ, Richardson BD, Handwerger S** 2001 Microarray analysis of trophoblast differentiation: gene expression reprogramming in key gene function categories. Physiol Genomics 6:105–116
11. **Cheng YH, Aronow BJ, Hossain S, Trapnell B, Kong S, Handwerger S** 2004 Critical role for transcription factor AP-2α in human trophoblast differentiation. Physiol Genomics 18:99–107
12. **Kudo Y, Boyd CA, Sargent IL, Redman CW, Lee JM, Freeman TC** 2004 An analysis using DNA microarray of the time course of gene expression during syncytialization of a human placental cell line (BeWo). Placenta 25:479–488
13. **Roh CR, Budhraja V, Kim HS, Nelson DM, Sadovsky Y** 2005 Microarray-based identification of differentially expressed genes in hypoxic term human trophoblasts and in placental villi of pregnancies with growth restricted fetuses. Placenta 26:319–328
14. **Chen B, Nelson DM, Sadovsky Y** 2006 *N*-myc down-regulated gene 1 modulates the response of term human trophoblasts to hypoxic injury. J Biol Chem 281:2764–2772
15. **Tanaka TS, Jaradat SA, Lim MK, Kargul GJ, Wang X, Grahovac MJ, Pantano S, Sano Y, Piao Y, Nagaraja R, Doi H, Wood 3rd WH, Becker KG, Ko MS** 2000 Genome-wide expression profiling of mid-gestation placenta and embryo using a 15,000 mouse developmental cDNA microarray. Proc Natl Acad Sci USA 97:9127–9132
16. **Galaviz-Hernandez C, Stagg C, de Ridder G, Tanaka TS, Ko MS, Schlessinger D, Nagaraja R** 2003 Plac8 and Plac9, novel placental-enriched genes identified through microarray analysis. Gene 309:81–89
17. **Hemberger M, Cross JC, Ropers HH, Lehrach H, Fundele R, Himmelbauer H** 2001 UniGene cDNA array-based monitoring of transcriptome changes during mouse placental development. Proc Natl Acad Sci USA 98:13126–13131
18. **Drey EA, Kang MS, McFarland W, Darney PD** 2005 Improving the accuracy of fetal foot length to confirm gestational duration. Obstet Gynecol 105:773–778
19. **American College of Obstetricians and Gynecologists** 1999 Practice bulletin 10. Induction of labor. Washington, DC: American College of Obstetricians and Gynecologists
20. **Haimov-Kochman R, Fisher SJ, Winn VD** 2006 Modification of the standard Trizol-based technique improves the integrity of RNA isolated from RNase-rich placental tissue. Clin Chem 52:159–160
21. **Auer H, Lyianarachchi S, Newsom D, Klisovic MI, Marcucci G, Kornacker K** 2003 Chipping away at the chip bias: RNA degradation in microarray analysis. Nat Genet 35:292–293
22. **Gentleman RC, Carey VJ, Bates DM, Bolstad B, Dettling M, Dudoit S, Ellis B, Gautier L, Ge Y, Gentry J, Hornik K, Hothorn T, Huber W, Iacus S, Irizarry R, Leisch F, Li C, Maechler M, Rossini AJ, Sawitzki G, Smith C, Smyth G, Tierney L, Yang JY, Zhang J** 2004 Bioconductor: open software development for computational biology and bioinformatics. Genome Biol 5:R80
23. **Bolstad BM** 2004 Low Level analysis of high-density oligonucleotide array data: background, normalization and summarization. Dissertation, University of California, Berkeley
24. **Smyth GK** 2005 Limma: linear models for microarray data. In: Gentleman RC, Carey V, Duboit R, Irizarry W, Huber, ed. Bioinformatics and computational biology solutions using R and Bioconductor. New York: Springer; 397–420
25. **Tibshirani R, Walther G, Hastie T** 2001 Estimating the number of clusters in a data set via the gap statistic. J R Stat Soc Series B 63:411–423
26. **Damsky CH, Fitzgerald ML, Fisher SJ** 1992 Distribution patterns of extracellular matrix components and adhesion receptors are intricately modulated during first trimester cytotrophoblast differentiation along the invasive pathway, *in vivo*. J Clin Invest 89:210–222
27. **Hertzel AV, Bennaars-Eiden A, Bernlohr DA** 2002 Increased lipolysis in transgenic animals overexpressing the epithelial fatty acid binding protein in adipose cells. J Lipid Res 43:2105–2111
28. **Wheeler DL, Barrett T, Benson DA, Bryant SH, Canese K, Chetvernin V, Church DM, DiCuccio M, Edgar R, Federhen S, Geer LY, Helmberg W, Kapustin Y, Kenton DL, Khovayko O, Lipman DJ, Madden TL, Maglott DR, Ostell J, Pruitt KD, Schuler GD, Schriml LM, Sequeira E, Sherry ST, Sirotkin K, Souvorov A, Starchenko G, Suzek TO, Tatusov R, Tatusova TA, Wagner L, Yaschenko E** 2006 Database resources of the National Center for Biotechnology Information. Nucleic Acids Res 34:D173–180
29. **Altschul SF, Madden TL, Schaffer AA, Zhang J, Zhang Z, Miller W, Lipman DJ** 1997 Gapped BLAST and PSI-BLAST: a new generation of protein database search programs. Nucleic Acids Res 25:3389–3402
30. **Eswar N, John B, Mirkovic N, Fiser A, Ilyin VA, Pieper U, Stuart AC, Marti-Renom MA, Madhusudhan MS, Yerkovich B, Sali A** 2003 Tools for comparative protein structure modeling and analysis. Nucleic Acids Res 31:3375–3380
31. **Sali A, Blundell TL** 1993 Comparative protein modelling by satisfaction of spatial restraints. J Mol Biol 234:779–815
32. **Pieper U, Eswar N, Braberg H, Madhusudhan MS, Davis FP, Stuart AC, Mirkovic N, Rossi A, Marti-Renom MA, Fiser A, Webb B, Greenblatt D, Huang CC, Ferrin TE, Sali A** 2004 MODBASE, a database of annotated comparative protein structure models, and associated resources. Nucleic Acids Res 32:D217–D222
33. **McGuffin LJ, Jones DT** 2003 Improvement of the GenTHREADER method for genomic fold recognition. Bioinformatics 19:874–881
34. **McLean M, Smith R** 1999 Corticotropin-releasing hormone in human pregnancy and parturition. Trends Endocrinol Metab 10:174–178
35. **Petraglia F, Calza L, Garuti GC, Abrate M, Giardino L, Genazzani AR, Vale W, Meunier H** 1990 Presence and synthesis of inhibin subunits in human decidua. J Clin Endocrinol Metab 71:487–1492
36. **Drake PM, Red-Horse K, Fisher SJ** 2004 Reciprocal chemokine receptor and ligand expression in the human placenta: implications for cytotrophoblast differentiation. Dev Dyn 229:877–885
37. **Collins JE, Goward ME, Cole CG, Smink LJ, Huckle EJ, Knowles S, Bye JM, Beare DM, Dunham I** 2003 Reevaluating human gene annotation: a second-generation analysis of chromosome 22. Genome Res 13:27–36
38. **Wyatt SM, Kraus FT, Roh CR, Elchalal U, Nelson DM, Sadovsky Y** 2005 The correlation between sampling site and gene expression in the term human placenta. Placenta 26:372–379
39. **Sood R, Zehnder JL, Druzin ML, Brown PO** 2006 Gene expression patterns in human placenta. Proc Natl Acad Sci USA 103:5478–5483
40. **Kinoshita T, Shirai K, Itoh M** 2003 The level of pre-heparin serum lipoprotein lipase mass at different stages of pregnancy. Clin Chim Acta 337:153–156
41. **Huter O, Wolf HJ, Schnetzer A, Pfaller K** 1997 Lipoprotein lipase, LDL receptors and apo-lipoproteins in human fetal membranes at term. Placenta 18:707–715
42. **Reese-Wagoner A, Thompson J, Banaszak L** 1999 Structural properties of the adipocyte lipid binding protein. Biochim Biophys Acta 1441:106–116
43. **Zimmerman AW, Veerkamp JH** 2002 New insights into the structure and function of fatty acid-binding proteins. Cell Mol Life Sci 59:1096–1116
44. **Smith AJ, Sanders MA, Thompson BR, Londos C, Kraemer FB, Bernlohr DA** 2004 Physical association between the adipocyte fatty acid-binding protein and hormone-sensitive lipase: a fluorescence resonance energy transfer analysis. J Biol Chem 279:52399–52405
45. **Tan NS, Shaw NS, Vinckenbosch N, Liu P, Yasmin R, Desvergne B, Wahli W, Noy N** 2002 Selective cooperation between fatty acid binding proteins and peroxisome proliferator-activated receptors in regulating transcription. Mol Cell Biol 22:5114–5127
46. **Okada S, Shimizu T, Yokotani K** 2003 Brain phospholipase C and diacylglycerol lipase are involved in corticotropin-releasing hormone-induced sympatho-adrenomedullary outflow in rats. Eur J Pharmacol 475:49–54
47. **Krensky AM** 2000 Granulysin: a novel antimicrobial peptide of cytolytic T lymphocytes and natural killer cells. Biochem Pharmacol 59:317–320
48. **Raychaudhuri SP, Jiang WY, Raychaudhuri SK, Krensky AM** 2004 Lesional T cells and dermal dendrocytes in psoriasis plaque express increased levels of granulysin. J Am Acad Dermatol 51:1006–1008

49. **King A, Loke YW, Chaouat G** 1997 NK cells and reproduction. Immunol Today 18:64–66
50. **Levine RJ, Karumanchi SA** 2005 Circulating angiogenic factors in preeclampsia. Clin Obstet Gynecol 48:372–386
51. **Zhou Y, Bellingard V, Feng KT, McMaster M, Fisher SJ** 2003 Human cytotrophoblasts promote endothelial survival and vascular remodeling through secretion of Ang2, PlGF, and VEGF-C. Dev Biol 263:114–125
52. **Xu X, Lee J, Stern DF** 2004 Microcephalin is a DNA damage response protein involved in regulation of CHK1 and BRCA1. J Biol Chem 279: 34091–34094
53. **Evans PD, Gilbert SL, Mekel-Bobrov N, Vallender EJ, Anderson JR, Vaez-Azizi LM, Tishkoff SA, Hudson RR, Lahn BT** 2005 Microcephalin, a gene regulating brain size, continues to evolve adaptively in humans. Science 309:1717–1720
54. **Khong TY, Liddell HS, Robertson WB** 1987 Defective haemochorial placentation as a cause of miscarriage: a preliminary study. Br J Obstet Gynaecol 94:649–655
55. **Michel MZ, Khong TY, Clark DA, Beard RW** 1990 A morphological and immunological study of human placental bed biopsies in miscarriage. Br J Obstet Gynaecol 97:984–988
56. **Kaufmann P, Black S, Huppertz B** 2003 Endovascular trophoblast invasion: implications for the pathogenesis of intrauterine growth retardation and preeclampsia. Biol Reprod 69:1–7
57. **Kim YM, Bujold E, Chaiworapongsa T, Gomez R, Yoon BH, Thaler HT, Rotmensch S, Romero R** 2003 Failure of physiologic transformation of the spiral arteries in patients with preterm labor and intact membranes. Am J Obstet Gynecol 189:1063–1069

***Endocrinology* is published monthly by The Endocrine Society (http://www.endo-society.org), the foremost professional society serving the endocrine community.**